Impact of Distributed Photovoltaic Generation and Customer Loads on Power Quality of a Distribution System

by

Titiksha Vijay Joshi

A Thesis Presented in Partial Fulfillment
of the Requirements for the Degree
Master of Science

Approved October 2014 by the
Graduate Supervisory Committee:

Gerald T. Heydt, Chair
Raja Ayyanar
Vijay Vittal

ARIZONA STATE UNIVERSITY

December 2014

ABSTRACT

There has been a considerable growth in distributed photovoltaic (PV) generation and its integration in electric power distribution systems. This has led to a change in the distribution system infrastructure. Properly planned distributed generation can offer a variety of benefits for system operations and enhance operational performance of the distribution system. However, high penetration of PV resources can give rise to operating conditions which do not arise in traditional systems and one of the potential issues that needs to be addressed involves impact on power quality of the system with respect to the spectral distortion in voltages and currents.

The test bed feeder model representing a real operational distribution feeder is developed in OpenDSS and the feeder modeling takes into consideration the objective of analysis and frequency of interest. Extensive metering infrastructure and measurements are utilized for validation of the model at harmonic frequencies. The harmonic study performed is divided into two sections: study of impact of non-linear loads on total harmonic voltage and current distortions and study of impact of PV resources on high frequency spectral distortion in voltages and currents. The research work incorporates different harmonic study methodologies such as harmonic and high frequency power flow, and frequency scan study. The general conclusions are presented based on the simulation results and in addition, scope for future work is discussed. Appendix A describes the general MATLAB code to perform high frequency power flow study.

ACKNOWLEDGMENTS

I would like to express my gratitude to my advisor, Dr. Gerald T. Heydt for his constant encouragement and support throughout the project. His invaluable insight and guidance has helped me immensely in my research work. I would also like to sincerely thank Dr. Raja Ayyanar and Dr. Vijay Vittal for their advice and helpful feedback in the project. I am happy to have had an opportunity of working with them and it has been a great learning experience for me.

I would like to acknowledge and thank the United States Department of Energy and Arizona Public Service for their support and financial assistance under contract DE-EE0004679. I would also like to thank Ms. Yingying Tang and Mr. Adarsh Nagarajan for guiding me with the software and providing all the important data to conduct this research.

Finally, and most importantly, I would like to sincerely and gratefully thank my parents, Mr. Vijay Joshi and Mrs. Sangita Joshi for their faith, unwavering love, continuous motivation, and support. My thanks also go to my friends and colleagues for their unending encouragement and love.

TABLE OF CONTENTS

Page

LIST OF TABLES v

LIST OF FIGURES vii

NOMENCLATURE ix

CHAPTER

1. AN OVERVIEW OF DISTRIBUTED PHOTOVOLTAIC GENERATION AND ITS INTEGRATION IN AN ELECTRIC DISTRIBUTION NETWORK 1

1.1 Growth of Renewable Energy in the United States 1

1.2 Distributed PV Generation in Distribution Systems 2

1.3 Thesis Objectives 5

1.4 Organization of Thesis 6

1.5 Non-Fundamental Frequency Components Present in Distribution System 7

2. MODELING AND VALIDATION OF THE TEST BED FEEDER 13

2.1 A Brief Description of the Test Bed Feeder 13

2.2 Modeling of the Test Bed Distribution Feeder in OpenDSS 14

2.3 An Overview of OpenDSS 23

2.4 Base Model of the Test Bed Feeder in OpenDSS 24

2.5 Harmonic Power Flow Algorithm Used in the Study 25

2.6 Validation of the Test Bed Distribution Feeder Model 28

CHAPTER Page

3. IMPACT OF NON-LINEAR LOADS ON POWER QUALITY OF THE TEST BED FEEDER 43

3.1 Harmonic Sources 43

3.2 Harmonic Load Modeling 44

3.3 Measurements Related to Harmonic Distortion 45

3.4 Harmonic Analysis in OpenDSS 49

3.5 Frequency Scan Study 55

3.6 Summary 59

4. IMPACT OF PV RESOURCES ON POWER QUALITY OF THE TEST BED FEEDER 60

4.1 The Inverter Interface for PV Systems 60

4.2 PWM Inverters 61

4.3 Details of the PV Systems Installed on the Test Bed Feeder 64

4.4 High Frequency Power Flow Simulations and Results 68

4.5 Analysis 75

5. CONCLUSIONS AND FUTURE WORK 78

5.1 General Conclusions 78

5.2 Future Work 80

REFERENCES 83

APPENDIX

A. GENERAL MATLAB CODE FOR HIGH FREQUENCY POWER FLOW STUDY 88

LIST OF TABLES

Table Page

2.1 Power Quality Meter Measurements 14

2.2 Comparison of Simulated Fundamental Voltages and Currents With Measurements 31

2.3 Test Bed Feeder Results for Third Harmonic Using Zone Division Method ..36

2.4 Test Bed Feeder Results for Fifth Harmonic Using Zone Division Method ...37

2.5 Test Bed Feeder Results for Seventh Harmonic Using Zone Division and Random Injection Current Method 38

2.6 Test Bed Feeder Results for Ninth Harmonic Using Zone Division and Random Current Injection Method 39

3.1 Steady State Power Flow Results.....52

3.2 Measured and Simulated Values of Voltage and Current THDs at Feeder DAS Locations.....52

4.1 Total Load and PV Generation in the Test Bed Feeder.....68

4.2 Voltage and Current THDs at Feeder DAS Locations.....70

4.3 Maximum Individual Voltage Distortion at All the High Frequencies 71

4.4 Voltage and Current THDs at Feeder DAS Locations.....73

4.5 Maximum Individual Voltage Distortion at All the High Frequencies 73

4.6 Maximum Individual Voltage Distortion for Current Injections With Random Phase Angles at 12 kHz 77

Table Page

4.7 Maximum Individual Voltage Distortion for Current Injections With Random Phase Angles at 16 kHz 77

LIST OF FIGURES

Figure Page

2.1 Feeder Diagram: A Test Bed for Examining Harmonics and High Frequency Components in a Distribution System With High PV Penetration 16

2.2 Distributed Parameter Model of a Transmission Line With Characteristic Impedance Z_c and Propagation Constant γ. The Lumped Parameters are Indicated As Impedances. 17

2.3 Lumped Parameter Model of a Distribution Transformer With Winding-Winding Capacitances Shown 20

2.4 Load Modeling for Harmonic Analysis 22

2.5 Internal Architecture of OpenDSS 24

2.6 Power Flow Solution Method 27

2.7 Reactive Power at Feederdas05 Monitored on July 1, 2013.....30

2.8 The Zone Division Method.....33

3.1 Locations of Feeder DAS Meters.....46

3.2 Variation in Voltage THD Over a Day at the Feeder DAS Locations.....47

3.3 Variation in Voltage THD in All Three Phases at FeederDAS01 47

3.4 Individual Harmonic Currents Measured from 12:00 A.M.-1:00 A.M. 48

3.5 Individual Harmonic Currents Measured from 12:00 P.M.-1:00 P.M.....49

3.6 Variation in Voltage THD Starting from Substation Till the End of Feeder...53

3.7 Positive Sequence Impedance Response at the Bus With Capacitor Bank 56

3.8 Zero Sequence Impedance Response at the Bus With Capacitor Bank.....56

3.9 Positive Sequence Impedance Response at Line Close to the Capacitor Bank57

Figure Page

3.10 Zero Sequence Impedance Response at Line Close to the Capacitor Bank ..57

4.1 Single Phase Full-Bridge Inverter..... 63

4.2 Percent Magnitude of High Frequency Spectral Current Component for Different Operating Levels of PV System 67

4.3 Voltage Profile Along the Test Bed Feeder.....69

4.4 Voltage Profile Along the Test Bed Feeder.....72

4.5 Impedance Magnitude and Phase Angle Response for Zero Sequence Current Injection 74

4.6 Impedance Magnitude and Phase Angle Response for Positive Sequence Current Injection 75

NOMENCLATURE

AC	Alternating current
AMI	Automated Metering Infrastructure
ASD	Adjustable speed drive
ATP	Alternative Transients Program
B	Susceptance
C_{hl}	High-to-low voltage winding capacitance
C_{hg}	High-to-ground winding capacitance
C_{lg}	Low-to-ground winding capacitance
COM	Computer Object Model
DAS	Data acquisition system
DC	Direct current
DER	Distributed energy resource
DF	Distortion factor
DG	Distributed generation
EPRI	Electric Power Research Institute
EMTP	Electromagnetic Transients Program
f_s	Inverter switching frequency in Hz
f_1	Fundamental frequency in Hz
h	Harmonic number
h_r	Resonant harmonic number

HV	High voltage
I_1	Fundamental current
I_h	Harmonic current
I_{peak}	Peak current
I_{rms}	Root mean square current
I1	Phase A current
I2	Phase B current
I3	Phase C current
$ITHD$	Current THD
IGBT	Insulated Gate Bipolar Transistor
$Iinj$	Injection current vector
IEEE	Institute of Electrical and Electronics Engineer
$I_{h\_total\_zone}$	Total harmonic current in a zone
$I_{fundamental\_total\_zone}$	Total fundamental current in a zone
I_{h_load}	Harmonic load current
I_{1_load}	Fundamental load current
LC	Inductor-capacitor
LV	Low voltage
MVA_{SC}	System short circuit MVA
$MVAr_{cap}$	Capacitor bank rating
m_a	Amplitude modulation ratio

m_f	Frequency modulation ratio
MOSFET	Metal Oxide Field Effect Transistor
NREL	National Renewable Energy Laboratory
OpenDSS	Open Source Distribution System Simulator
P	Real power
PV	Photovoltaic
PWM	Pulse Width Modulation
RLC	Resistor-Inductor-Capacitor
R-L	Resistance-Inductance
r_0	Zero sequence line resistance
r_1	Positive sequence line resistance
RMS	Root Mean Square
R_c	Transformer core resistance
R_{eq}	Transformer equivalent leakage resistance
THD	Total Harmonic Distortion
TIF	Telephone Influence Factor
UL	Underwriters Laboratories
V_1	Fundamental voltage
V_h	Harmonic voltage
VBA	Visual Basic
V_a, V1	Phase A voltage
V_b,V2	Phase B voltage

V_c,V3	Phase C voltage
X_m	Transformer magnetizing reactance
x_0	Zero sequence line reactance
x_1	Positive sequence line reactance
X	Reactance
X_{eq}	Transformer equivalent leakage reactance
Y_s	Long-line shunt admittance
Y	Line admittance per unit length
Z	Line impedance per unit length
Z_s	Long-line series impedance
Z_c	Characteristic impedance
Z_0	Zero sequence source impedance
Z_1	Positive sequence source impedance
ω	Angular frequency in rad/s
γ	Propagation constant
θ_h	Harmonic current phase angle
θ_1	Fundamental current phase angle
$\theta_{hspectrum}$	Harmonic spectrum phase angle at h
$\theta_{1spectrum}$	Harmonic spectrum phase angle at h=1

CHAPTER 1

AN OVERVIEW OF DISTRIBUTED PHOTOVOLTAIC GENERATION AND ITS INTEGRATION IN AN ELECTRIC DISTRIBUTION NETWORK

1.1 Growth of Renewable Energy in the United States

Generation from renewable resources is increasing in response to calls for sustainable energy, and aggressive renewable portfolio standard mandates. Also, the use of renewable resources is in response to federal tax credits, grants, and a variety of other state and local policies such as rebates, tax incentives, financing assistance. In addition, environmental impact of fossil fired plants, rising prices of fossil fuels, increasing CO_2 emissions and search for clean source of energy has led to investment in developing power conversion technologies for generation from renewable resources. During the time frame 2008 to 2012, the United States doubled its electricity generation from renewable resources using a combination of wind, solar and geothermal technologies [1]. In the year 2012, 12.4% of the net electricity generation in United States (TWh) came from the renewable resources including conventional hydropower, wind, biomass, geothermal, and solar. Hydropower and wind constituted 6.8% and 3.4% of the net electric generation in United States respectively and the grid-connected photovoltaic (PV) systems contributed to 0.3% of the total electric generation [1]. The grid-connected PV is growing consistently since enactment of federal and state policies and continues to increase in market share. According to the NREL report, the net installed PV capacity in United States reached 2.5 GW by the end of 2010. Of the total installed PV capacity of 2.5 GW, an estimate of 2.1 GW was grid-connected [2].

1.2 Distributed PV Generation in Distribution Systems

The majority of distribution systems are radially configured. Before the integration of distributed generation, the radial design insured that active power flowed from the distribution substation head through the distribution feeder to the end-users. With the proliferation of distributed generation at customer sites and the integration of distributed resources with the grid, there is a shift in the distribution system infrastructure from centralized to distributed generation. Distributed energy resource (DER) systems are generally small scale power generation sources (e.g., <10 kW) providing an alternative to the traditional electric power distribution system to meet the load demand. These resources cover a wide range, from fuel cells, steam turbines, microturbines to renewable resources like wind turbines, photovoltaic systems. Distributed PV generation consists of roof-top and utility scale large PV resources.

Residential roof-top PV installations comprises of few solar panels and are typically relegated to 2-5 kW while the large utility scale PV system can be in the range of 100 kW and above. Though the installation costs are high, several government subsidies, financial assistance and long-term benefits associated with PV have encouraged installation of solar panels in the residential areas. Smaller-scale residential and commercial projects account for the majority of grid-connected PV capacity. According to the U.S. Energy Information Administration's Short Term Energy Outlook Report, the utility scale PV capacity doubled in 2013 and a continued growth in solar electricity generation with concentration in customer-sited installations is expected [3].

A. Potential benefits of distributed PV generation

Properly planned distributed generation (DG) can provide a variety of benefits for system operations, such as improved operational performance of the grid, increased system reliability and financial savings. Detailed analysis of benefits associated with distributed generation can be found in [4-8]. In summary, the specific areas of benefits are highlighted below:

- Increased electric system reliability - Several utilities offer incentives to DG owners to shed demand during system needs (demand response), declare units as emergency units to make them available during times of system need ensuring system adequacy and reliability [5], [6].
- Reduction of peak power requirements and deferral in T&D investments - In some cases, addition of distributed generation can reduce peak load requirements and lower the power delivery costs as substitute or deferral of new distribution investments. DG unit can help serve the load locally during peak demand, reducing the system losses. Reduction in peak demand can reduce wear and tear of equipment, reducing maintenance costs and improving system life [4], [8].
- Provision of ancillary services - DG installments can help in providing local voltage improvement and control, and reactive power support [7].

B. Problems with distributed PV generation

High penetration of PV generation can give rise to operating conditions which do not arise in conventional systems and some of the potential problems which need detailed analysis are as follows:

- Distributed generation at the end user and commercial sites can cause shift in the power flow pattern through the system. The reversal in power flow can cause problems like over-voltage, incorrect operation of voltage regulators, and inaccurate capacitor switching [9-11].
- It can cause misoperation of protection circuit like circuit breakers, relays, fuses and create problems with traditional fuse-fuse, fuse-recloser coordination, leading to possible islanding of small part of the system. Unless the system is carefully designed for intentional islanded operation, unintentional islanding places the system at risk for a number of reasons including equipment damage, overvoltage [12-14].
- It can lead to power quality problems such as increase in voltage unbalance due to uneven distribution of single phase PV units, and increase in spectral injections in the grid [15].

As described above, deployment of distributed PV resources in the distribution feeder can have adverse effects on the system power quality and reliability. The issues related to integration of PV resources will not always occur but addressing these issues and its assessment becomes important if reliability and power quality of the system has to be maintained. The performance of a distribution

feeder with PV resources added will depend on the PV penetration level, feeder electrical characteristics, location of PV systems, system control settings, and the configuration of the system. IEEE Standard 1547 provides a set of criteria and requirements related to the performance, operation, safety, and maintenance of interconnection of distributed generation to the grid. The cited standard provides details for issues such as allowable voltage drop, short circuit currents, and voltage flicker [16].

1.3 Thesis Objectives

The aim of this research is to study the impact of distributed PV resources and customer loads on the power quality of the feeder. The presence of non-linear electronic loads and addition of PV resources will lead to increasing spectral injection in the grid. Harmonic currents generated by a large number of single phase electronic loads present in the feeder along with larger loads like adjustable speed drives (ASDs) can cause appreciable distortion in grid voltage. These non-linear loads are injectors of low order (baseband) harmonic currents. In the study reported here, the baseband harmonics are relegated to well below 25^{th} harmonic of 60 Hz (1500 Hz). The reason for confinement of the harmonic voltages and currents are based on several factors including the limited bandwidth of the distribution system, and also the limited harmonic content of typical distribution system loads. PV systems, on the other hand, generate high frequency current spectral components (e.g., > 2 kHz) which propagate in the system to cause distortion. Modern PV inverters employ various pulse width modulation (PWM) technologies as an

interface to distribution systems thus improving power conversion efficiency and generating power with greater flexibility and control [17],[18],[24]. The frequency spectrum at the output voltage of the PV inverter consists of large component at fundamental frequency and high frequency components. This research investigates the distortion in voltages and currents in the distribution feeder due to the low order baseband harmonics as well as high frequency components that exist in the system.

The distribution system selected for study is the actual system in the state of Arizona and instrumented measurements are available. Modeling of the feeder which is appropriate for harmonic and high frequency analysis and its validation has been accomplished in OpenDSS, an open source simulation tool developed by the Electric Power Research Institute (EPRI) [19]. Impact of baseband harmonics and high frequency components on the distribution feeder operation has been analyzed for various scenarios. Harmonic study methodologies like frequency scan, harmonic and high frequency power flow are implemented to investigate the effect on power quality of voltages and currents in the feeder.

1.4 Organization of Thesis

The thesis is divided into a total of five chapters. Chapter 1 builds a background on integration of distributed PV resources into the distribution networks and their operational impacts. Chapter 2 describes modeling of the test bed feeder and various feeder components in OpenDSS for harmonic and high frequency analyses. The two methods used for feeder validation are explained and their re-

sults are discussed in Chapter 2. Chapter 3 focuses on investigating the effect of non-linear loads on power quality of the feeder with respect to voltage and current distortion while Chapter 4 studies the high frequency spectral distortion in the feeder voltages and currents caused by the PV resources. The calculation of high frequency spectral components and results for high frequency power flow study are presented in Chapter 4. Chapter 5 summarizes the important conclusions, contributions and in addition, scope for future work is discussed.

Appendix A describes the general MATLAB code developed to conduct high frequency power flow study.

1.5 Non-Fundamental Frequency Components Present in Distribution System

The non-fundamental frequency components present in the distribution network, serving mostly residential load and with PV systems installed, can be divided into two categories: harmonics (i.e., at integer multiples of the fundamental frequency up to 3 kHz) and high frequency components which result from electronic switching (generally above 2 kHz).

A. Harmonics and their impact

Widely distributed single phase non-linear loads are a source of harmonics in distribution systems. Most of these loads employ capacitor-filtered bridge rectifiers and use diodes, silicon-controlled rectifiers (SCRs), and other switching devices to convert AC to DC or to chop waveforms to control power. The harmonic sources can be classified into switch mode power supplies used in computers, televisions, rectifiers used in DC motor drives, battery chargers and inverters in ad-

justable speed drives. Other harmonic sources not related to power electronics include transformers' magnetic saturation, fluorescent lamps, DC electric arc furnaces [20].

Harmonic distortion is a major cause of power quality problems. High levels of harmonic distortion can cause several ill-effects such as conductor overheating due to increased currents, increased heating and damage of equipment such as transformers, capacitors, motors, increase in system losses, interference with telephone circuits, incorrect meter readings, misoperation of protective relays, and faulty operation of electronic equipment which depend on and are sensitive to waveshape [21]. The overall efficiency of utilization of electrical energy is reduced. The ill-effects are more pronounced if resonant conditions occur.

The inductive reactance of the electric system elements increases and the capacitive reactance decreases with increase in the harmonic order. At some frequency, there will be a crossover point where the inductive and capacitive reactances are equal. The phenomenon is called as resonance and it results in amplification of harmonic currents and voltages in the system. These amplified voltages and currents are observed in the system if the harmonic frequency produced by a non-linear load coincides with the natural frequency of the system. The presence of capacitor banks in the system can cause resonance, leading to its damage due to excessive heating [21]. There are two types of resonance:

- Parallel resonance offers high impedance at resonant frequency and since harmonic sources are considered as current sources, this results in in-

creased harmonic voltages. Capacitor banks in parallel with the system impedance can give rise to parallel resonance [20].

- Series resonance occurs when a harmonic source sees inductance, in form of transformer or equivalent system, in series with capacitor. It offers low impedance path to the harmonic current at resonant frequency [20].

Harmonics can be classified based on the frequency and phase sequence. Harmonic sequence refers to the phase sequence of the harmonic voltages and currents with respect to the fundamental phasors in a three phase four-wire balanced system. Assuming a balanced three phase system, harmonics of different orders will form the following sequence set:

- Harmonics of order 1, 4, 7, 10,... are positive sequence.
- Harmonics of order 2, 5, 8, 11,... are negative sequence.
- Harmonics of order 3, 6, 9, 12,... are zero sequence.

If a system is not balanced, then each harmonic can have positive, negative, and zero sequence components.

B. Distortion indices

Distortion in voltages and currents can be quantified using Total Harmonic Distortion (THD). It is the ratio of root mean square (RMS) value of harmonic current (or voltage) above fundamental frequency to the RMS value of fundamental current (or voltage). Total harmonic distortion (THD) is given by,

$$THD = \frac{\sqrt{\sum_{h=2}^{N} I_h^2}}{I_1} \tag{1.1}$$

The distortion factor (DF) is the individual voltage or current harmonic distortion. It is calculated as a percentage of fundamental voltage or current component and is given by,

$$DF = \frac{V_h}{V_1} \tag{1.2}$$

IEEE 519 recommends guidelines for harmonic control and provides limits for total current and voltage distortion along with individual harmonic current and voltage distortion limits [22]. For operating voltage of 69 kV and below, the recommended limit for individual voltage distortion is 3% and total voltage distortion limit is 5%. IEEE 519 is a system standard widely used in North America.

Two other measures of distortion are crest factor and form factor given as,

$$Crest\ factor = \frac{I_{peak}}{I_{RMS}} \tag{1.3}$$

$$Form\ factor = \frac{I_{RMS}}{I_1}. \tag{1.4}$$

Other indices such as telephone interference factor (TIF) and I•T product are used to measure telephone interference.

C. High frequency spectral components and their impacts

Many PV inverters employ pulse width modulation technology to convert DC power into controlled AC power output. Pulse width modulation strategies use semiconductor switches such as MOSFETs, IGBTs capable of switching at high frequencies. It offers advantages like flexible control of output power and frequency, smaller filter size, and lower electromagnetic interferences. As the switching frequency of these inverters is in the range of 2 kHz and above, the PV inverters generate high frequency current components, which are superimposed

on the power frequency (60 Hz) current. In effect, the spectral distortion in the frequency range up to 2 kHz is reduced [23-24].

Note these high frequency components are not termed ‘harmonics’ as they are not integer multiples of fundamental frequency, that is, 60 Hz.

With increasing power electronics interfaces, the high frequency current components injected in the distribution systems will increase. These high frequency currents will propagate depending on the system damping and they can be attenuated at the inverter output terminals using LC filter [26]. However, presence of these high frequency signals can impact the power network and installed electrical equipments. Some of the negative impacts of the high frequency current and voltage components include deterioration in performance of electronic equipments, interference with communication networks, and reduced service life of equipments. An important concern with accumulation of high frequency spectral current components is the possibility of triggering a resonant mode in the system leading to high amplitude of voltages and currents. An investigation of this issue requires detailed analysis and development of precise network models. Under certain circumstances, it may cause cable insulation damage and cable failure [27].

The Underwriters Laboratories standard UL 1741 covers the requirements for PV modules and inverters to provide AC output power for stand-alone uses or utility-interaction [28]. The UL standards are mainly written for safety and insurance adjustor purposes. As the PV inverters are grid-connected, these requirements should be used in conjunction with IEEE 1547. IEEE 1547 provides the guidelines for interconnecting the distributed resources with the electric power

systems [16]. These standards specify the guidelines to control noise and harmonic content in the inverter systems and ensure inverters do not generate excessive spectral distortion which can contaminate AC supply voltage. As the PV generation in the system increases, the utilities are concerned about the impact of PV inverter spectral distortion on the power quality of the grid.

CHAPTER 2

MODELING AND VALIDATION OF THE TEST BED FEEDER

2.1 A Brief Description of the Test Bed Feeder

To adequately determine the effects of distributed energy resources for a distribution system and to carry out a study of the voltage, current, and power flow, it is important to have distributed generation at a scale where the impacts are measurable and data can be acquired with sufficient detail through proper instrumentation and monitoring infrastructure. In this case, an actual distribution feeder is used. The test feeder selected for study is an operational feeder located in northern Arizona. The distribution primary is approximately 10 miles long. It has a minimum load of about 3 MW and the historical peak load is about 7 MW. The total PV deployment on this feeder accounts for 1.5 MW which gives relatively high peak penetration and this level of PV penetration is sufficient to demonstrate its impact on the power quality of the test bed feeder. There are a total of 125 residential roof-top PV resources distributed throughout the artifact feeder and these roof-top PV resources are rated between 2 and 4 kW. In addition, there are two large scale three phase PV systems installed at two different locations, one at about 3 miles and other at 7 miles from the substation. These utility scale PV resources are rated 400 kW and 700 kW respectively. The feeder serves approximately 2,700 residential and 300 commercial customers. The modeling of the test bed distribution feeder in OpenDSS is presented in detail in the following section.

Several types of data acquisition prototypes are developed and installed on the test bed feeder to collect information related to the PV system operations, and feeder performance. Automated metering infrastructure (AMI) is used to record hourly energy consumption by customer loads and PV generation from all the sites every 15 minutes. Further, power quality meters are installed at 17 different PV sites to record a full range of power quality parameters at their output terminals. Electrical parameters related to the primary feeder are obtained from 6 different locations using power quality meters. These meters record individual current and voltage harmonics present in the feeder. A list of measurements from the power quality meter is given in Table 2.1. The RMS values are recorded. The metered values give the total effective voltages and currents including harmonics.

Table 2.1 Power Quality Meter Measurements

Phase voltage	Phase current	Line-to-line voltage
Apparent power	Active power	Reactive power
Power factor	Current THD	Voltage THD
Frequency	Voltage deviation	Frequency deviation
Long term voltage flicker	Short term voltage flicker	

2.2 Modeling of the Test Bed Distribution Feeder in OpenDSS

Distribution systems are generally radial and often unbalanced. The unbalanced nature is due to the appearance of single phase laterals and loads. A full three phase representation of the feeder is used for conducting power flow and harmonic analysis. The loads can be categorized as either linear or harmonic-producing non-linear loads.

The circuit model consists of a 12.47 kV three phase primary, branching out into single and double phase laterals along the feeder. These laterals terminate at distribution transformers which step down the voltage to 120 V/277 V to serve the customer loads. Figure 2.1 shows the distribution feeder diagram for the test bed in detail. The 12.47 kV three phase primary is shown in heavy black. The phases A, B, and C are separated in single phase laterals. Distribution of residential roof-top PVs along with large scale PV systems is marked by circles. Residential roof-top PVs are connected to the secondary of distribution transformers at 120 V/277 V while the large three phase PV systems are connected to the three phase primary either directly or through a transformer. A total of three capacitor banks are installed on the feeder for voltage regulation and are indicated by the arrows in the Figure 2.1.

The modeling of different feeder components takes into account the frequency of interest and type of studies to be performed. OpenDSS circuit includes modeling of overhead and underground lines, transformers, capacitor banks, substation source, loads, and PV systems.

A. Capacitor banks

Three wye-connected capacitor banks are modeled in OpenDSS. Two of these capacitor banks are voltage controlled, located at the middle and end of feeder with ratings of 600 kVAr each. The third capacitor bank is current controlled, located at the substation and is rated at 1200 kVAr.

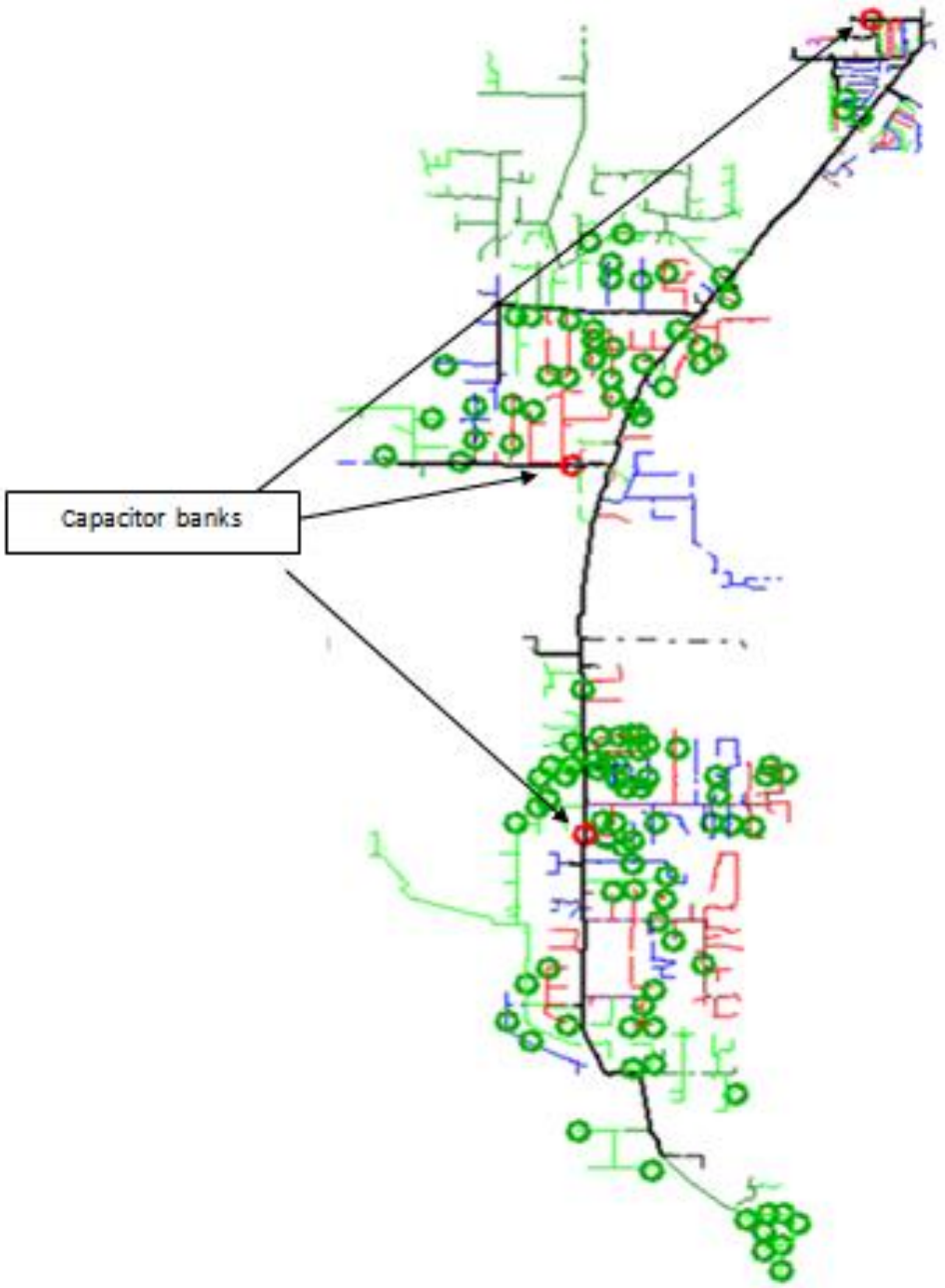

Figure 2.1 Feeder Diagram: A Test Bed for Examining Harmonics and High Frequency Components in a Distribution System With High PV Penetration

B. Overhead and underground lines

The three phase overhead line is modeled as a three phase balanced line, assuming it is transposed. The overhead and underground lines are modeled as multiphase equivalent π-models using positive and zero sequence impedance data. For analysis considering low order harmonics up to 25th harmonic, this modeling suffices but for the frequency in range of 2 kHz and above, the long-line effect of line sections is considered (i.e., the distributed parameter model is used, and this results in a partial differential equation model) [29]. Figure 2.2 shows the long-line π model of a transmission line with characteristic impedance *Zc* and propagation constant γ at frequency ω. These parameters are given by,

$$Z_c = \sqrt{\frac{Z}{Y}} \tag{2.1}$$

$$\gamma = \sqrt{ZY} \tag{2.2}$$

where *Z* and *Y* are the unit length transmission line impedance and admittance respectively (at frequency ω).

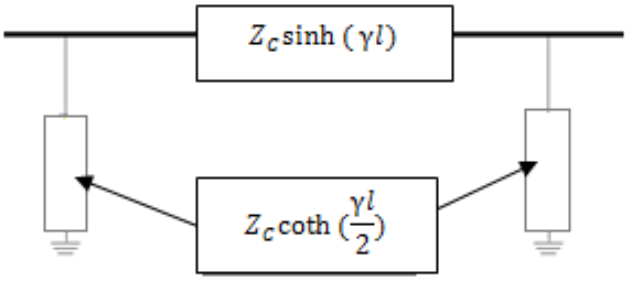

Figure 2.2 Distributed Parameter Model of a Transmission Line With Characteristic Impedance Z_c and Propagation Constant γ. The Lumped Parameters are Indicated As Impedances.

The distributed parameter model is 'exact' at one frequency, namely ω. The 'derivation' of Figure 2.2 appears in [30] and this derivation is found by writing and solving the partial differential equations for a transmission line on uniform *Z* and *Y*.

OpenDSS calculates the distributed parameters of a single phase line section automatically for any specified frequency. This is proved by comparing the line impedances computed by OpenDSS with distributed line parameters of different line sections calculated in MATLAB. To illustrate this, consider an overhead single phase line with length of 0.5249 miles. The sequence impedances given to OpenDSS are r_0=2.3015 ohm/mile, r_1=1.69 ohm/mile, x_1= 0.9312 ohm/mile, x_0= 2.4998 ohm/mile. The long-line parameters are calculated in MATLAB.

For the cited example, the series impedance of the long-line section is given by

$$Z_s = Z_c \, sinh(\gamma l) = 0.8871 + j\, 0.4888 \text{ ohms}$$

The shunt admittance is calculated using

$$Y_s = \frac{Y\gamma l}{2tanh(0.5\gamma l)} = \text{-1.0743e-22} + j\, 1.3560\text{e-06 siemens}$$

The capacitance in each parallel branch = 3.42619 nF.

The series impedance and shunt admittance calculated by OpenDSS are compared with the MATLAB calculations and the values are found to be accurate up to four digits after the decimal point. For the three phase lines, the entire feeder length is divided into line sections of short lengths and these line sections are then

connected in series. This design takes into account the distributed parameter modeling of line.

Another important issue is the skin effect of lines. Due to skin effect, the conductor resistance increases with an increase in frequency. It has been observed that skin effect can be ignored for common low order harmonic assessment problems [25]. However, for analyses involving high frequencies (in kHz), the skin effect will be considerable and to represent this phenomenon in the feeder model, all the overhead and underground lines are defined based on line geometries and conductor configurations. OpenDSS computes the line sequence impedances internally including the skin effect at each specified frequency.

C. Transformers

Transformers are the power delivery elements modeled as equivalent T-circuits. Most of the distribution transformers are rated at 25 kVA. Y-grounded/Y-grounded winding configuration has been assumed for all the 921 transformers. The HV and LV winding voltages, kVA rating, equivalent winding reactance and resistance are provided as input to OpenDSS. At normal operating frequency, the effect of parasitic capacitance between turns and layers of windings is negligible and thus ignored in the modeling of transformer. At frequencies above 4 kHz, the effect of stray capacitances is noticeable and they are represented as lumped capacitances between the windings, namely, high-to-low voltage winding (C_{hl}), high-to-ground (C_{hg}) and low-to-ground winding capacitances (C_{lg}) [31], [32]. Figure 2.3 shows a lumped parameter model of a distribution trans-

former with core resistance and magnetizing reactance (R_c, X_m) and leakage resistance and reactance (R_{eq}, X_{eq}).

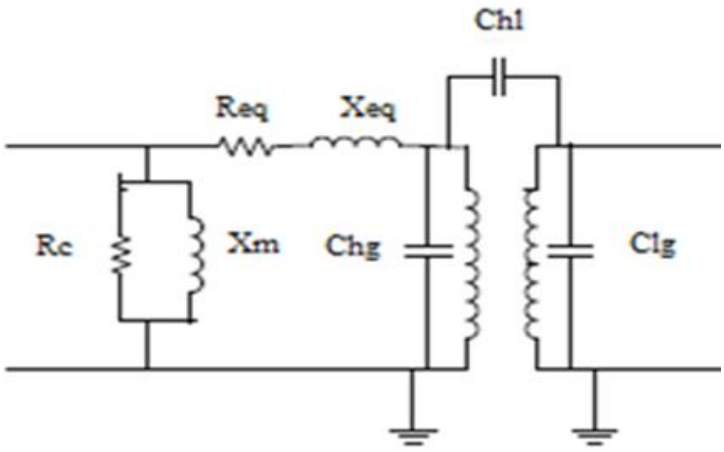

Figure 2.3 Lumped Parameter Model of a Distribution Transformer With Winding-Winding Capacitances Shown

The values of lumped capacitances will majorly depend on the specific winding design and to a very less extent on the voltage and kVA rating of the transformer. Using the notation 'H' for the high side, and 'L' for the low side, typical ranges of the lumped capacitances are provided below:

- H-ground capacitance is between 1 and 2 nF.
- H-L capacitance is between 2 and 6 nF.
- L-ground capacitance is between 5 and 10 nF.

The transformer modeling to represent the transformer behavior for a wide bandwidth frequency is presented in [33] and the simulation results are confirmed from actual frequency response analysis (FRA) test measurements.

D. Loads

The residential and commercial loads served by the test bed feeder are typically a mix of linear and non-linear loads. All the loads served by a common secondary winding of a distribution transformer are aggregated and applied as a spot load at the transformer secondary. For 60 Hz analysis, a constant *PQ* model is used to represent load and the active and reactive power data is obtained from automated metering infrastructure. All the loads are entered separately as a single phase load.

For the harmonic analysis based on current injection method, load is modeled as a Norton equivalent circuit where current source represents the harmonic currents injected by non-linear portion of the load and do not possess any RLC model. The shunt admittance is used to represent the linear load and is a combination of series *R-L* and parallel *R-L*. The linear portion of the load provides a damping element to harmonic propagation.

Figure 2.4 shows a Norton equivalent model of a load element in OpenDSS. The current source is set to the value of fundamental current times the multiplier defined in the 'spectrum' object associated with the load for the frequency being solved. The equivalent shunt admittance can be adjusted by stating the percentage of linear load that is connected as series *R-L* and parallel *R-L* where *B* and *X* are frequency dependant.

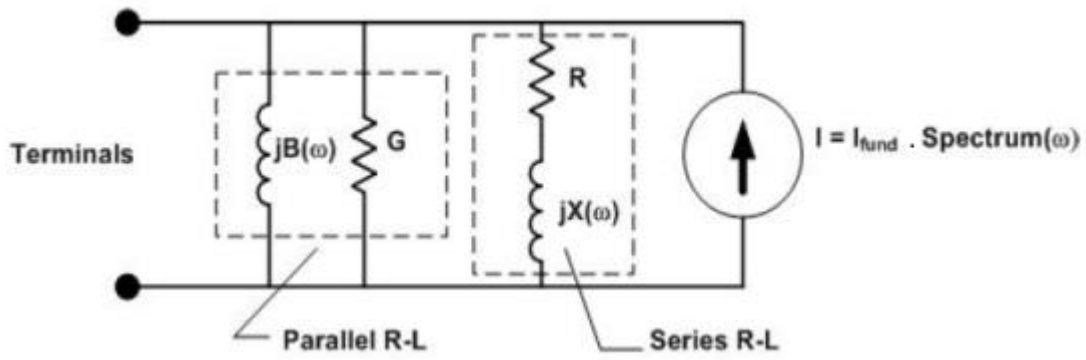

Figure 2.4 Load Modeling for Harmonic Analysis [36]

E. PV systems

There are a total of 125 single phase roof-top PV units connected to the secondary of service transformers at 120 V. The utility scale three phase PV systems are connected to the three phase primary either directly or through a 480 V/12.47 kV transformer. The reactive power control for the two large PV units is not considered in this study. Also, the distributed roof-top PV units are not allowed to perform active voltage regulation [16]. The PV systems can be modeled as generators providing active power at unity power factor. Alternatively, for the harmonic study, the PV units are modeled as loads with negative active power operating at unity power factor. A current source is modeled at each of the PV site to inject the high frequency spectral components generated by PV resources. Amplitudes and phase angles of the high frequency spectral components are identified and are associated with the 'Isource' object in OpenDSS. The PV generation profile is obtained from AMI.

F. Equivalent source at the substation

Substation voltage is monitored and depending on the time of snapshot simulation, the three phase voltages can be obtained from substation data acquisition system (DAS). The equivalent impedance looking from the low voltage side of substation transformer is measured and this impedance is given as:

- Positive sequence impedance, $Z_1 = 0.1000 + j\ 1.1023$ ohms
- Zero sequence impedance, $Z_0 = 0.0507 + j\ 0.8440$ ohms

2.3 An Overview of OpenDSS

OpenDSS [34] is an open source software developed by the Electric Power Research Institute (EPRI). The software is designed to support modeling of balanced or unbalanced, multi-phase electric power distribution systems and it performs several types of utility distribution system analysis. OpenDSS is based on frequency domain. Harmonic analysis is one of the main capabilities of this tool and harmonic simulation can be performed on complicated circuits quite easily [35]. In addition, OpenDSS can perform sequential time simulations called 'quasi-static' solutions. This feature can be used to perform daily, yearly, and duty cycle simulations. OpenDSS is a script-driven simulation engine and it has a feature of Windows Computer Object Model (COM) interface where programs like MATLAB, VBA Excel can access the program features and drive simulator to perform new types of studies [36].

The internal architecture of OpenDSS software is shown in Figure 2.5. The DSS Executive stores global variables and options; it has one circuit object

which consists of five classes of circuit elements and a solution depending upon the solution mode selected [36].

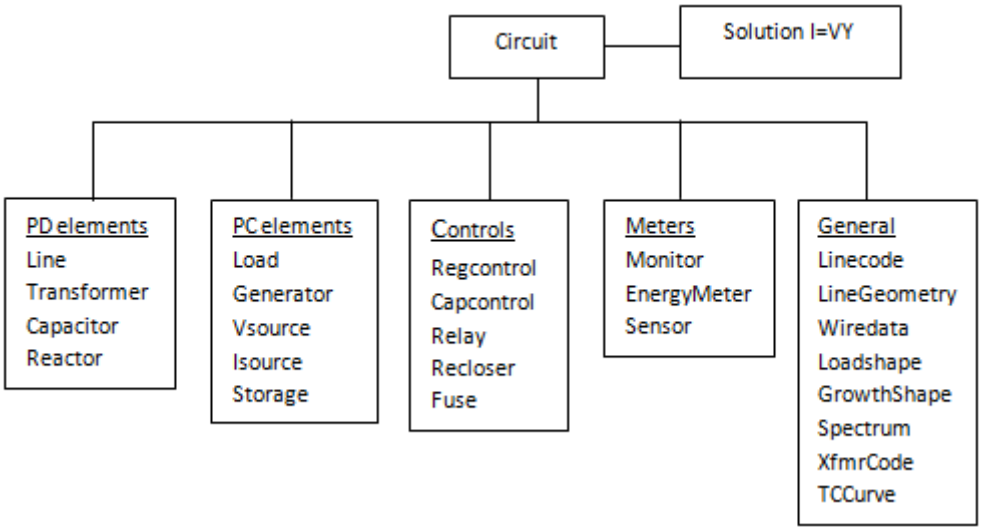

Figure 2.5 Internal Architecture of OpenDSS [36]

2.4 Base Model of the Test Bed Feeder in OpenDSS

The test bed distribution feeder modeled in OpenDSS consists of about 4000 nodes, 921 transformers and 107 PV systems. The complete circuit model includes a total count of about 10 files, each file defining details of specific model elements. The basic input files that are always required for the study irrespective of the type of analysis are:

- Line section definition
- Transformer definition
- Capacitor data and control configuration
- PV generation data
- Load data

- Bus coordinates.

Additional input files are called based on the objective of study. For the harmonic analysis, line code definition file specifying the line sequence impedances is included. For high frequency analysis, the additional input files required are:

- Line geometry definition
- Wire data definition for overhead lines
- Concentric neutral cable definition for underground cables
- Transformer winding capacitances definition.

All the input files required for analysis are specified in the Master.dss file. The initial step is to compile the script in OpenDSS by creating Run.dss file. The Run.dss file provides a path for Master.dss file, and the list of feeder parameters that are to be exported for further analysis. The feeder parameters can be phase voltages or line voltages at each node, currents in each element, power transferred in each element or system losses.

2.5 Harmonic Power Flow Algorithm Used in the Study

Different approaches have been proposed and implemented to solve the harmonic power flow problems. The procedures for analyzing the harmonic problems can be classified into time-domain, frequency-domain and hybrid time-frequency domain approaches. Time domain approaches are based on transient analysis and electromagnetic transient programs such as EMTP/ATP have been used [29]. One disadvantage is that long computation time might be required for

especially large power systems. Frequency domain methods are widely used for harmonic problem formulations and analysis. The frequency domain method calculates the frequency response of the system and requires shorter computation time [20], [30].

A. Power flow algorithm in OpenDSS

Steady state power flow is used to determine the static system operating conditions; it calculates the network bus voltages at fundamental frequency from the constraints of power and/or voltage. This is the first step to initialize harmonic solution. The two basic types of power flow solution used in OpenDSS are iterative power flow and direct solution [38]. The default is iterative power flow where the power conversion elements like loads, distributed generators are treated as injection sources. The power flow algorithm can be explained as follow:

1) Calculate the initial values of bus voltages for iteration for no load condition, by forming the network admittance matrix and without considering any power conversion element.

2) Include all the power conversion elements in the network by calculating the injection current, *Iinj* and associated admittance matrix from the node voltage and power of each power conversion element.

3) Build the injection current matrix by using injection currents from all the power conversion elements. Node voltages can be calculated with the injection current matrix and the system admittance matrix through matrix operation as shown in Figure 2.6. Keep iterating the above steps until the error in node voltages falls within tolerance limit [38].

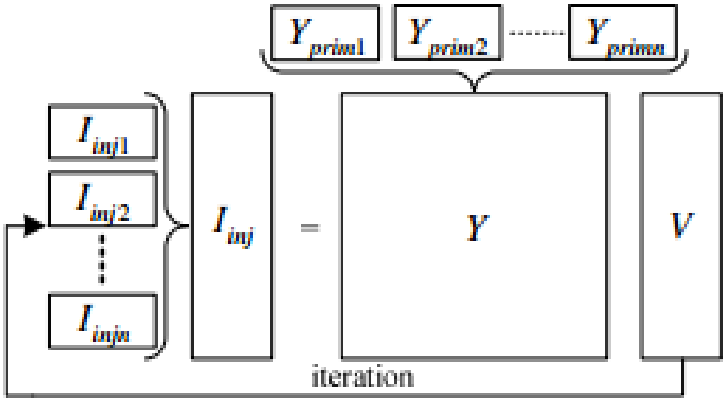

Figure 2.6 Power Flow Solution Method [38]

B. Decoupled harmonic power flow in OpenDSS

Once the conventional power flow converges, harmonic mode is initialized. OpenDSS implements a decoupled harmonic power flow algorithm, where it builds the linear admittance matrix at each of the frequency specified in the program and uses a direct solution to solve for voltages and currents throughout the system at all the specified frequencies [20], [38]. The harmonic study involves solving for the node voltages at each harmonic using the network equation given by,

$$[I_h] = [Y_h][V_h] \qquad h=1,2,\ldots,N \tag{2.3}$$

where I_h is the vector of source currents, Y_h is the nodal admittance matrix, V_h is the vector of bus voltages, h is the harmonic order. The notation N refers to the maximum harmonic order of interest (e.g., 13^{th} harmonic, but IEEE 519 recommends 83^{rd} harmonic).

The harmonic power flow method in OpenDSS is from a class of nodal admittance matrix harmonic solution tools. The harmonic power flow solution methods and formulations have been discussed in [39].

The non-linear loads are modeled as decoupled harmonic sources that inject harmonic currents into the system which are initialized to proper magnitudes and phase angles based on the fundamental power flow solution and harmonic spectrum associated with them. The harmonic current magnitude is assumed to be a percentage of fundamental load current. The phase relationship between the fundamental current and non-linear element used to calculate the harmonic phase angle is given by

$$\theta_h = \theta_{hspectrum} + h(\theta_1 - \theta_{1spectrum}\ ) \tag{2.4}$$

where h is the harmonic number, θ_h is the phase angle of current injected at harmonic h, $\theta_{hspectrum}$ is the phase angle specified in the harmonic spectrum at harmonic h, θ_1 is the fundamental current phase angle and $\theta_{1spectrum}$ is the phase angle displacement at fundamental frequency given in the spectrum [40]. The 'monitor' object can be used to capture the harmonic voltages and currents at any specific location in the circuit. The results can be exported to other programs for further analysis.

2.6 Validation of the Test Bed Distribution Feeder Model

Once the test bed feeder model is developed in OpenDSS, it is necessary to validate the model at fundamental and harmonic frequencies. Individual harmonic current and voltage measurements are available at six locations on the three

phase primary and these measurements are used in the feeder validation process. The six monitoring locations are referred as feederDAS01, feederDAS02, feederDAS03, feederDAS04, feederDAS05, and feederDAS06.

The load data, harmonic currents and voltages up to and at 15^{th} harmonic available at 1:00 A.M. on July 1, 2013 are used for model validation. The required load data is obtained from AMI.

A. Power flow simulation results

Substation voltage is continuously monitored by the substation data acquisition system. For the time being considered, the measured values are V_a= 1.0417 p.u.; V_b= 1.04 p.u.; V_c= 1.0418 p.u.

The power flow is solved in OpenDSS and simulated voltages and currents at feeder DAS locations are compared with the measured voltages and currents. The challenge in this task is the unknown status of capacitor banks. Different combinations of capacitor banks are used to solve the power flow and simulation results are compared with the measurements. The status of two voltage controlled capacitor banks located at the middle and end of the feeder is confirmed by analyzing the reactive power profile at feederDAS05. Figure 2.7 shows the reactive power at feederDAS05 location for July 1, 2013. The switching of the two capacitor banks along the feeder is reflected in the form of step rise or fall in the reactive power flow at feederDAS05. A step rise (or fall) of 200 kVAr in Figure 2.7 indicates switching off (or on) of one of the capacitor banks where 200 kVAr is the per phase rating of both the capacitor banks. Similarly, feeder DAS at the substation reflects the operation of current controlled capacitor bank located at the

substation. From the analysis, it is observed that the capacitor banks along the feeder are switched off and the capacitor bank at the substation is switched on.

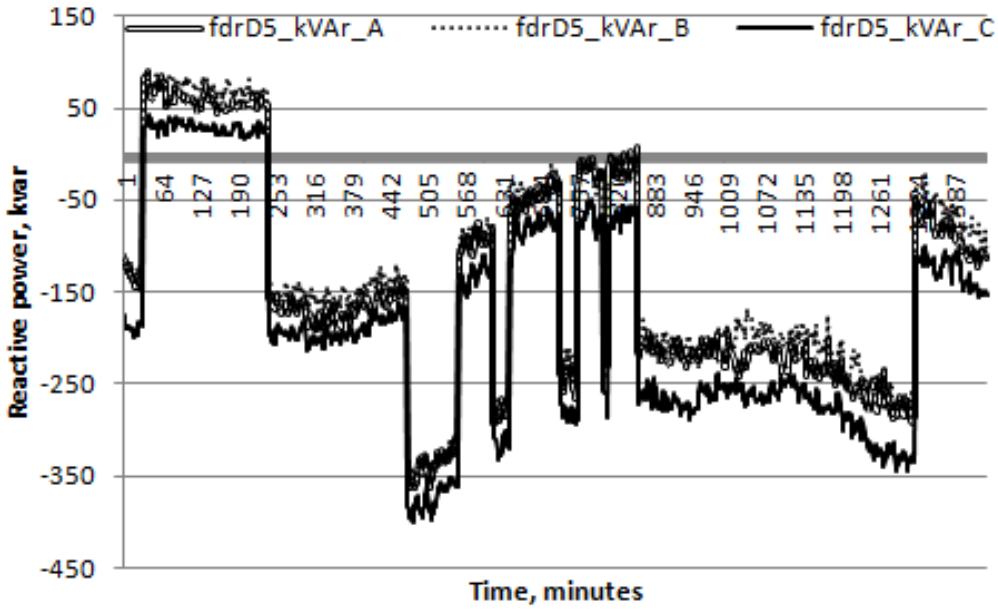

Figure 2.7 Reactive Power at Feederdas05 Monitored on July 1, 2013

Table 2.2 shows a comparison of power flow simulation results with actual measurements at the feeder DAS locations. The difference in the simulated and measured phase voltage increases towards the end of the feeder.

For the test bed feeder model validation at harmonic frequencies, two methods are implemented, namely zone division method and random current injection method (RCI). The details of the feeder validation methods are explained in the following sections.

Table 2.2 Comparison of Simulated Fundamental Voltages and Currents With Measurements

Location	V1 (kV)	V2 (kV)	V3 (kV)	I1 (Amp)	I2 (Amp)	I3 (Amp)
feederDAS06						
Simulated	7.319	7.328	7.336	187.505	174.8	167.982
Measured	7.459	7.457	7.451	148.79	124.03	137.38
feederDAS05						
Simulated	7.116	7.138	7.205	85.0078	83.0431	63.6588
Measured	7.392	7.406	7.38	70.72	69.96	53.154
feederDAS04						
Simulated	7.06	7.102	7.181	10.0276	7.04313	4.39542
Measured	7.375	7.374	7.37	7.7	5.87	3.45
feederDAS03						
Simulated	6.968	7.034	7.127	51.1175	30.2513	36.4848
Measured	7.351	7.344	7.345	45.33	35.24	27.3
feederDAS02						
Simulated	6.91	7.021	7.099	35.3554	14.3334	14.6129
Measured	7.31	7.342	7.318	28.49	14.57	12.28
feederDAS01						
Simulated	6.878	6.99	7.075	2.78668	6.41485	6.55383
Measured	7.311	7.33	7.287	2.48	5.63	5.38

B. Zone division method

The feeder is divided into five zones as shown in Figure 2.8. The loads and transformers in each zone are identified. The zones are formed in such a way such that each zone encloses a feeder DAS. Using harmonic current measurements from the feeder DAS locations and fundamental currents from the power flow solution, harmonic currents injected by all the loads in each zone are calculated. The total harmonic current ($I_{h\_total\_zone}$) and total fundamental current ($I_{fundamental\_total\_zone}$) in each zone is calculated by subtracting the downstream DAS value from the upstream DAS value.

The calculation for total harmonic and total fundamental currents in any zone can be expressed mathematically as,

$$I_{h\_total\_zone} = I_{upstreamDAS\_measured} - I_{downstreamDAS\_measured} \quad (2.5)$$

$$I_{fundamental\_total\_zone} = I_{upstreamDAS\_simulated} - I_{downstreamDAS\_simulated} \quad (2.6)$$

All the loads are assumed to be a source of harmonic currents. With this assumption, the harmonic current contribution of each load in a given zone is based on the ratio of fundamental load current to the total fundamental current in the same zone and is given by

$$I_{h\_load} = \frac{I_{h\_total\_zone} * I_{1\_load}}{I_{fundamental\_total\_zone}} \quad (2.7)$$

where I_{h_load} is the magnitude of harmonic current injected by a load, I_{1_load} is the magnitude of the fundamental current of the same load.

There are no data available related to the harmonic spectral magnitude and phase angle of load harmonics present in the test bed feeder. The harmonic spectrum for each load is defined using magnitude component obtained from (2.7). The phase angle is taken to be zero degrees. The phase angle of fundamental voltage does not vary much from head to the end of feeder (simulation results show a maximum change of 3 degrees) and the low order harmonics produced by the loads will have similar phase relationship with fundamental voltage, thus, expecting minimum harmonic cancellation. The harmonic mode is then executed in OpenDSS to obtain harmonic voltages at all the nodes and harmonic currents in all the elements of the system.

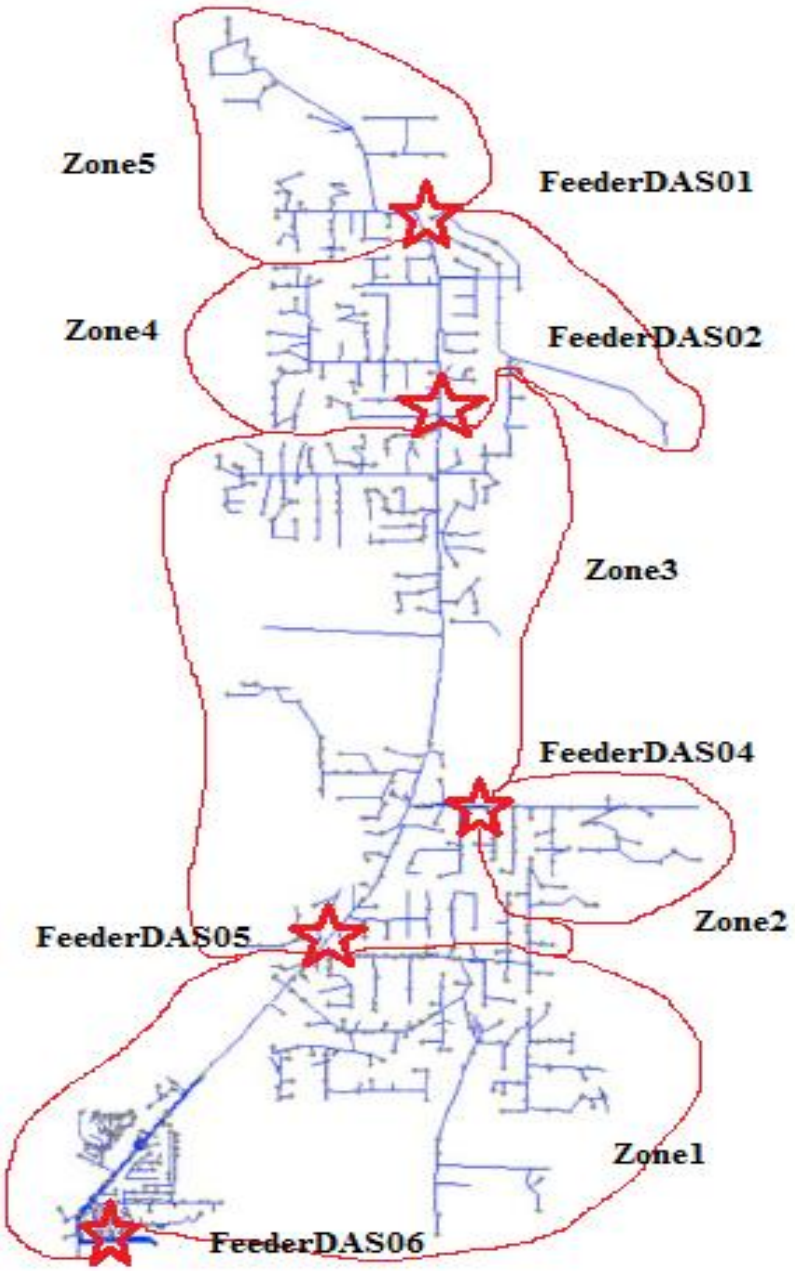

Figure 2.8 The Zone Division Method

Table 2.3-2.6 shows a comparison between simulated and measured values of voltages and currents at the six feeder DAS locations at harmonic frequencies up to the 9^{th} harmonic. The harmonic currents obtained from simulations match very well with the measurements at the 3^{rd} and 5^{th} harmonic. Some of the issues related to the zone division method are discussed below:

- In the zone division method, all the loads are assumed to inject harmonic currents proportional to their fundamental current. But in reality, this might not hold true. The loads that are actual sources of harmonics in the network, their placement and their true harmonic current contribution can potentially vary. Also, the presence of capacitor banks can affect the current distribution in the network and hence, the technique of allocating the total harmonic currents in a zone to individual loads directly based on the ratio might not be an effective method.
- There is no information on the phase angle of harmonic currents measured in the test bed feeder. The calculation of total harmonic current in each zone and the load harmonic spectrum is based on the arithmetic difference of the harmonic currents obtained from feeder DAS locations rather than phasor difference of harmonic currents which can be a possible reason for small offset in simulated currents.

Note that this method is used for the validation of feeder model up to and at 9^{th} harmonic as the harmonic currents measured above 9^{th} harmonic are insignificant.

C. Random current injection (RCI) method

In this method, zone-wise allocation of loads is used and the harmonic current injections from the loads are varied randomly in a uniform distribution manner. The upper bound for the magnitude of harmonic current injected is set by referring values obtained from zone division method; lower bound is set to zero. For harmonics of the order seven and above, phase angles of the individual load harmonic currents are widely distributed [42], [43]. The phase angle dispersion of individual current harmonics occurs due to the variation in power level, line impedance and *X/R* ratio [44]. This can lead to harmonic attenuation and cancellation. Therefore, the phase angle component of load spectrum is also varied randomly for the validation of test bed feeder at the 7^{th} and 9^{th} harmonic.

The process is executed in MATLAB which is used to drive harmonic simulations in OpenDSS and the method is used only for the 7^{th} and 9^{th} harmonic. The solution is obtained only when the simulated harmonic voltages and currents are within a good range of the measurements and the results should hold good at minimum five or all six feeder DAS locations. The maximum allowable error in voltages is set as 30% which is a reasonable choice as the maximum values of harmonic voltages measured in the test bed feeder are up to 200 V where the fundamental base voltage is 7.2 kV. Table 2.5-2.6 gives a comparison between simulated results and feeder DAS measurements.

Table 2.3 Test Bed Feeder Results for Third Harmonic Using Zone Division Method

Location	V1 (V)	V2 (V)	V3 (V)	I1 (Amps)	I2 (Amps)	I3 (Amps)
feederDAS06						
Measured	47.665	37.98	56.98	9.15	7.44	8.62
Simulated	50.9715	44.8876	52.407	8.36153	7.232	8.12602
% error	6.94%	18.18%	8.02%	8.61%	2.78%	5.73%
feederDAS05						
Measured	123.4	125.368	111.81	4.56	4.4	3.79
Simulated	143.614	136.789	143.721	4.17632	4.47021	3.85588
% error	16.38%	9.11%	28.54%	8.41%	1.59%	1.74%
feederDAS04						
Measured	126.41	145.938	151.045	0.638	0.446	0.17
Simulated	167.239	160.806	166.417	0.541239	0.453643	0.180082
% error	32.29%	10.18%	10.17%	15.16%	1.71%	5.93%
feederDAS03						
Measured	151.037	168.646	169.257	2.97	2.9	2.505
Simulated	202.381	198.592	202.239	2.50844	2.52027	2.45616
% error	33.99%	17.75%	19.48%	15.54%	13.09%	1.95%
feederDAS02						
Measured	181.34	158.754	186.176	1.91	1.37	1.12
Simulated	215.934	212.667	214.994	1.75487	1.79005	1.0973
% error	19.07%	33.96%	15.47%	8.12%	30.66%	2.03%
feederDAS01						
Measured	184.588	165.31	193.93	0.1949	0.495	0.59
Simulated	224.451	224.087	223.921	0.152193	0.745027	0.503443
% error	21.59%	35.56%	15.46%	21.90%	50.50%	14.67%

Table 2.4 Test Bed Feeder Results for Fifth Harmonic Using Zone Division Method

Location	V1 (V)	V2 (V)	V3 (V)	I1 (Amps)	I2 (Amps)	I3 (Amps)
feederDAS06						
Measured	68.23	85.27	78.13	7.37	5.96	5.92
Simulated	62.1084	51.5723	55.1195	7.3326	6.77072	6.47532
% error	8.97%	39.52%	29.45%	0.51%	13.60%	9.38%
feederDAS05						
Measured	113.65	109.66	121.87	3.96	4.49	3.64
Simulated	110.124	109.495	97.425	4.50071	5.57094	4.3104
% error	3.10%	0.15%	20.05%	13.65%	24.07%	18.42%
feederDAS04						
Measured	125.5	123.77	141.41	0.32	0.17	0.17
Simulated	120.84	129.45	108.498	0.304961	0.254449	0.225396
% error	3.71%	4.59%	23.27%	4.69%	49.67%	32.58%
feederDAS03						
Measured	140.46	140.4	140.19	2.78	2.85	2.34
Simulated	139.069	168.067	127.392	2.88705	3.13775	2.71473
% error	0.99%	19.70%	9.12%	3.85%	10.09%	16.01%
feederDAS02						
Measured	146.407	137.6	160.56	1.81	1.332	1.14
Simulated	147.746	180.998	133.284	2.03712	2.13924	1.26372
% error	0.91%	31.53%	16.98%	12.54%	60.60%	10.85%
feederDAS01						
Measured	152.72	139.48	162.29	0.24	0.41	0.53
Simulated	151.041	194.44	137.381	0.24	0.88	0.512813
% error	1.09%	39.40%	15.34%	1.97%	115.33%	3.24%

Table 2.5 Test Bed Feeder Results for Seventh Harmonic Using Zone Division and Random Injection Current Method

Location	V1 (V)	V2 (V)	V3 (V)	I1 (Amps)	I2 (Amps)	I3 (Amps)
feederDAS06						
Measured	44.36	44.848	60.5	1.76	1.04	1.649
Zone division	33.2694	35.1008	30.4924	2.39264	2.58695	2.06444
Random current inj	37.9462	33.8016	37.8536	2.61216	2.0808	2.10758
%error (zone div)	25%	21.73%	49.60%	35.94%	148.74%	25.19%
%error (RCI)	14.16%	24.63%	37.43%	48.18%	100.07%	27.81%
feederDAS05						
Measured	72.32	54.75	66.54	1.7078	1.27	0.926
Zone division	67.0449	69.2344	45.0984	2.3061	2.43807	1.3539
Random current inj	52.9789	55.2504	60.2745	0.90358	0.68005	0.75096
%error (zone div)	7.29%	26.45%	32.22%	35.03%	91.97%	46.21%
%error (RCI)	26.43%	0.91%	9.42%	47.09%	46.45%	18.90%
feederDAS04						
Measured	61.49	56.89	87.58	0.074	0.0327	0.0327
Zone division	77.9125	80.585	48.4371	0.08648	0.1332	0.0712
Random current inj	56.3091	57.9256	64.5073	0.05712	0.07977	0.05246
%error (zone div)	26.71%	41.65%	44.69%	16.86%	307.34%	118%
%error (RCI)	8.42%	1.82%	26.34%	22.82%	143.95%	60.43%
feederDAS03						
Measured	75.61	89.42	60.57	1.0877	0.69	0.6477
Zone division	97.4664	103.568	52.7766	1.51286	1.54962	0.81961
Random current inj	62.9029	62.8506	71.962	0.60244	0.4353	0.4667
%error (zone div)	28.90%	15.82%	12.86%	39.09%	124.58%	26.54%
%error (RCI)	16.81%	29.71%	18.80%	44.61%	36.91%	27.94%
feederDAS02						
Measured	93.59	70.49	71.36	0.795	0.415	0.25
Zone division	105.412	112.407	53.3699	1.04283	1.15954	0.31874
Random current inj	65.7138	64.9363	74.5462	0.46426	0.34689	0.13511
%error (zone div)	12.63%	59.46%	25.21%	31.17%	179.41%	27.49%
%error (RCI)	29.78%	7.87%	4.46%	41.60%	16.41%	45.95%
feederDAS01						
Measured	61.85	74.76	104.79	0.08	0.16	0.27
Zone division	108.058	122.86	53.4618	0.08576	0.60898	0.27606
Random current inj	66.1312	68.0435	75.9063	0.02441	0.25748	0.0633
%error (zone div)	74.71%	64.33%	48.98%	7.20%	280.61%	2.24%
%error (RCI)	6.92%	8.98%	27.56%	69.49%	60.92%	76.55%

Table 2.6 Test Bed Feeder Results for Ninth Harmonic Using Zone Division and Random Current Injection Method

Location	V1 (V)	V2 (V)	V3 (V)	I1 (Amps)	I2 (Amps)	I3 (Amps)
feederDAS06						
Measured	9.9	11.003	14.309	0.87	0.82	0.5295
Zone division	27.7876	60.1789	51.1381	0.59912	1.69551	1.12177
Random current inj	26.2556	22.6488	14.1534	0.76	0.632189	0.472527
%error (zone div)	180.68%	446.95	257.30%	31.13%	106.70%	111.85%
%error (RCI)	165.20%	105.84%	1.08%	12.64%	22.90%	10.75%
feederDAS05						
Measured	28.589	47.829	42.329	1.096	1.4288	1.13
Zone division	75.5345	125.303	95.9393	0.83587	1.89243	1.0162
Random current inj	49.8794	48.5751	36.1831	0.80631	0.582491	0.705448
%error (zone div)	164.21%	161.98%	126.60%	23.73%	32.44%	10.07%
%error (RCI)	74.47%	1.55%	14.51%	26.43%	59.23%	37.57%
feederDAS04						
Measured	61.44	67.04	44.48	0.1	0.0795	0.02
Zone division	91.6527	147.488	110.88	0.03925	0.163252	0.079591
Random current inj	57.8963	57.6242	44.6503	0.04377	0.074976	0.035749
%error (zone div)	49.17%	120%	149.20%	60.75%	105.34%	297%
%error (RCI)	5.76%	14.04%	0.38%	56.23%	5.69%	78.74%
feederDAS03						
Measured	86.98	71.887	95.23	1.07	1.099	0.95
Zone division	123.765	193.475	140.745	0.69687	1.69609	0.829911
Random current inj	80.5857	82.9858	66.8706	0.9087	0.954278	0.597041
%error (zone div)	42.29%	169.14%	47.79%	34.87%	54.33%	12.64%
%error (RCI)	7.35%	15.43%	29.77%	15.07%	13.16%	37.15%
feederDAS02						
Measured	85.27	100.514	111.398	0.906	0.698	0.4728
Zone division	136.831	213.721	152.62	0.6065	1.46778	0.34625
Random current inj	94.8715	99.3029	79.4487	0.94954	0.938531	0.380401
%error (zone div)	60.46%	112.62%	37%	33.05%	110.28%	26.76%
%error (RCI)	11.26%	1.20%	28.68%	4.80%	34.46%	19.54%
feederDAS01						
Measured	111.72	109.21	95.79	0.15	0.225	0.35
Zone division	146.378	234.957	160.525	0.14341	0.958776	0.296737
Random current inj	102.74	114.295	89.2013	0.09936	0.457148	0.254255
%error (zone div)	31.02%	115.14%	67.58%	4.39%	326.12%	15.21%
%error (RCI)	8.03%	4.65%	6.87%	33.76%	103.17%	27.35%

The following observations are made based on the feeder validation results:

- Results for the 3rd harmonic using zone division method show simulated currents are in a good agreement with measured currents with difference in currents being less than 0.5 A at almost all locations. The method is based on using the harmonic current measurements at feeder DAS locations to replicate the system behavior and conditions at each harmonic frequency and then observing harmonic voltages at monitored locations. The simulated harmonic voltages at the 3rd harmonic match well with measurements at the head of the feeder. The error between simulation values and measurements begins to increase towards the end of feeder and a maximum difference of 60 V is observed in phase B at the end of feeder.
- For the 5th harmonic, simulated harmonic voltages for phases A and C are in a good agreement with measurements and a maximum difference of 50 V is observed in phase B at the end of feeder. Simulated currents in phases A and C match with the measurements and the phase B currents show high error magnitudes at the end of feeder.
- Note that the base voltage at all the feeder DAS locations where harmonics are recorded is 7.2 kV (line-to-neutral voltage). The percentage errors presented in the above tables are calculated as percentage of harmonic measurements. The maximum mismatch in the harmonic voltages for 3th harmonic is 60 V, which will account for an error of 0.833% when ex-

pressed as a percentage of fundamental voltage. The difference is insignificant. Further, the maximum mismatch in harmonic voltages observed for the 5^{th} harmonic is less than the 3^{rd} harmonic.

- For the test feeder harmonic validation at the 7^{th} harmonic, use of the zone division method resulted in relatively higher values of simulated currents and voltages. This method calculates the total harmonic current in each zone based on arithmetic (not phasor) difference of harmonic currents obtained from feeder DAS and ignores the phase angle dispersion of individual load harmonics. Basically, the zone division method assumes no harmonic cancellation up to 9^{th} harmonic. The random current injection method incorporates the possibility of phase angle diversity contributed by individual load harmonics for harmonics of order 7 and above. The simulated currents at 7^{th} harmonic are observed to be lower than measured currents and the voltages are found to match well with the measurements. Random current injection method performs better as compared to the zone division method.
- For the 9^{th} harmonic case, the percentage error in phase B simulated currents is quite high at some locations in zone division method, and the error reduces when random current injection method is used. Also, the harmonic voltage values are better predicted by the random current injection method.

- The large mismatch observed in the currents for 7^{th} and 9^{th} harmonic at some locations in zone division method is due to the increase in currents in feeder line sections (including single phase laterals and three phase primary) contributed by the shunt capacitances of the lines. Many of these single phase laterals are underground cables with a large value of shunt capacitance (maximum number of underground cables seen in phase B). The shunt capacitive reactance of line decreases with an increase in harmonic order, the capacitive current increases and the current distribution in the network changes. As a result, allocation of total harmonic current in a zone to individual loads based on a direct ratio is not an effective method.
- Also, measurements show that the magnitudes of harmonic currents at 7^{th} and 9^{th} harmonic are quite low, maximum value being less than 2A and 1A respectively and a small deviation in simulation current from the actual measurement gives a large error.

Thus, feeder validation techniques are included in the study to check the accuracy and reliability of the feeder modeled in OpenDSS and it helps obtaining an improved base case model for power quality studies.

CHAPTER 3

IMPACT OF NON-LINEAR LOADS ON POWER QUALITY OF THE TEST BED FEEDER

3.1 Harmonic Sources

Prior to the advancement in power electronic devices, the main sources of current distortion were rectifiers, fluorescent lamps, DC electric arc furnaces and transformers to some extent. The increasing use of power electronics converter devices for the control of power is raising concern about current and voltage distortion in recent times. The common electronic loads used in domestic and office environment encompass switch mode power supplies used in computers, televisions, printers, rectifiers used in battery chargers, DC motor drives and inverters in adjustable speed drives [37]. Although the individual ratings of these devices can be small, the cumulative effect can result in appreciable grid distortion [41].

Many commercial and residential appliances require DC current for their operation. The single phase full-wave diode bridge rectifier is often employed owing to its light weight, compact size, reasonable cost and relatively low sensitivity to supply voltage distortion under normal operating conditions [20]. The diode bridge is directly connected to the AC line and input current waveform is characterized by a pulsed current which flows during the charging of capacitor placed at the DC side of rectifier. In an ideal case, harmonics and magnitude of the spectral components present in the AC current are given by,

$$h=nq \pm 1 \tag{3.1}$$

$$I_h = \frac{I_1}{h} \tag{3.2}$$

where h is the harmonic number, n is any positive integer, q is the pulse number of the rectifier circuit, I_h is the magnitude of harmonic current of order h, and I_1 is the magnitude of fundamental current. In a real case, the square wave is softened by the system inductance and typical values of harmonic currents for converters utilizing six or more pulses are provided in [22].

3.2 Harmonic Load Modeling

Most harmonic flow analysis on power systems are performed using steady state, linear circuit solution techniques. For nearly all analysis, most harmonic-producing loads can be represented as current injection sources. This representation is based on the assumption that the system supply voltage is not distorted and the modeling is quite accurate up to harmonic voltage distortion levels of 10% [46]. The total harmonic current content injected by the electronic devices can be determined using power quality meters. However, in absence of measurements, it is common to assume that harmonic current content is inversely proportional to the harmonic number. This is derived from the Fourier series for a square wave, which forms the foundation of many non-linear devices. However, it does not apply very well to the new technology PWM drives and switch-mode power supplies, which have a much higher harmonic content [37].

The constant current source method allows handling several harmonic sources simultaneously and gives the solution directly without any iteration. This method is reliable to analyze cases involving typical normal operating conditions.

In cases where the system is near resonance, a simple current source model will give an excessively high prediction of voltage distortion. The model tries to inject a constant current into a high impedance network, which is not a valid representation of reality. Advanced load modeling techniques include Norton equivalent and crossed frequency admittance matrix model [45]. The Norton model provides an additional impedance to moderate the parallel resonance response and can represents the load model accurately for different load and voltage cases.

3.3 Measurements Related to Harmonic Distortion

This section concentrates on the low order baseband current harmonics present in the test bed feeder and its contribution to total harmonic distortion in voltages. Four weeks of power quality data is collected from the six feeder DAS meters located on the three phase primary. Figure 3.1 shows the locations of the feeder DAS meters.

A. Variation in voltage and current THD

The power quality meters record total harmonic distortion in voltages and currents. Figure 3.2 shows the variation in voltage THD over an entire day at one minute interval captured at all the feeder DAS locations. The voltage THDs are measured in phase A on July 22, 2013. The following observations are made:

- The voltage THD at end of the feeder (feederDAS01 and feederDAS02) is always higher than the THD monitored at the upstream feeder DAS elements. The voltage THD decreases progressively along the three phase primary towards the head of feeder.

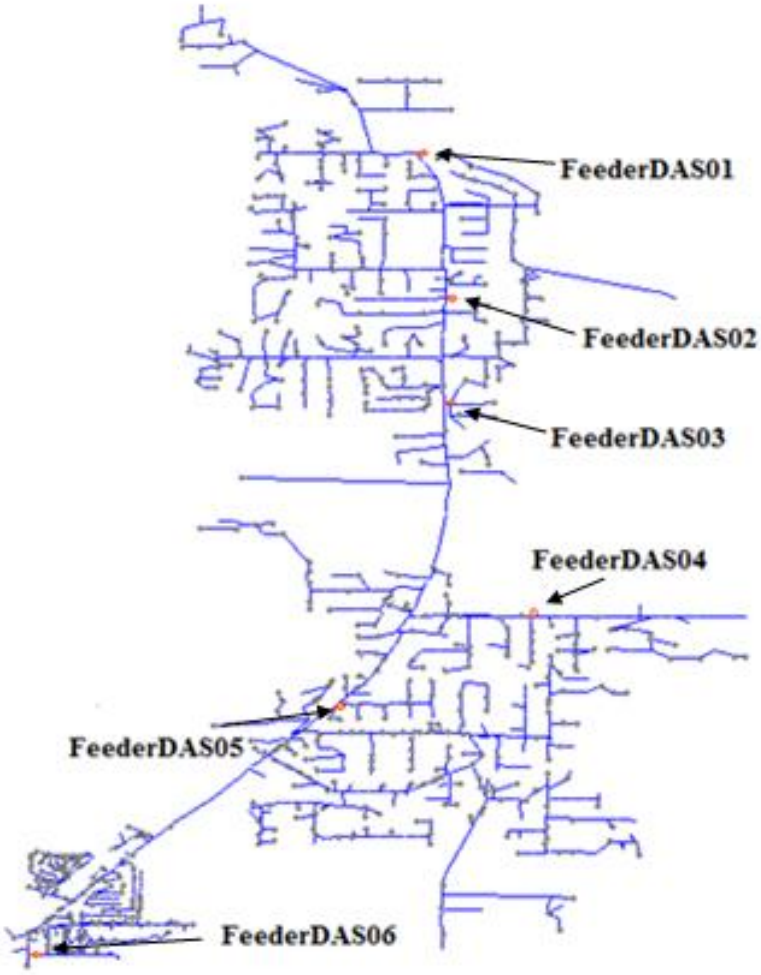

Figure 3.1 Locations of Feeder DAS Meters

- In the evening at around 19:00, the voltage THD rises and it is as high as 9%. The PV inverters are not operating during this period and the observed high amount of distortion can be attributed to prominent proportion of electronic loads present in the system. The feeder serves mostly residential loads and the period between 19:00 to 21:00 marks significant use of electronic loads like televisions, computers, and kitchen appliances.

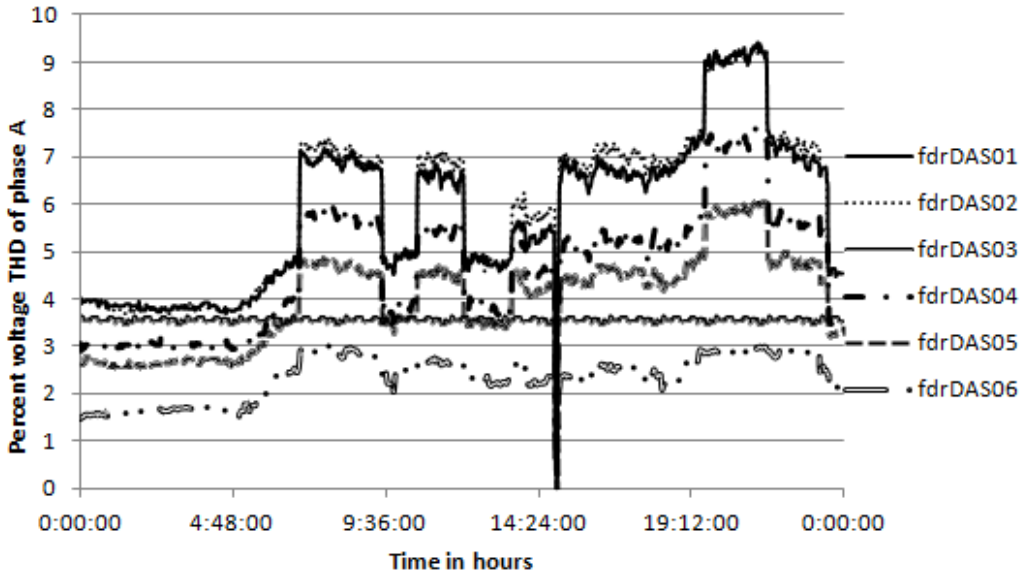

Figure 3.2 Variation in Voltage THD Over a Day at the Feeder DAS Locations

Figure 3.3 shows the variation in voltage THD in all three phases at feed-erDAS01 as seen on July 22, 2013 and it is found that the variation in voltage THD is similar in all three phases.

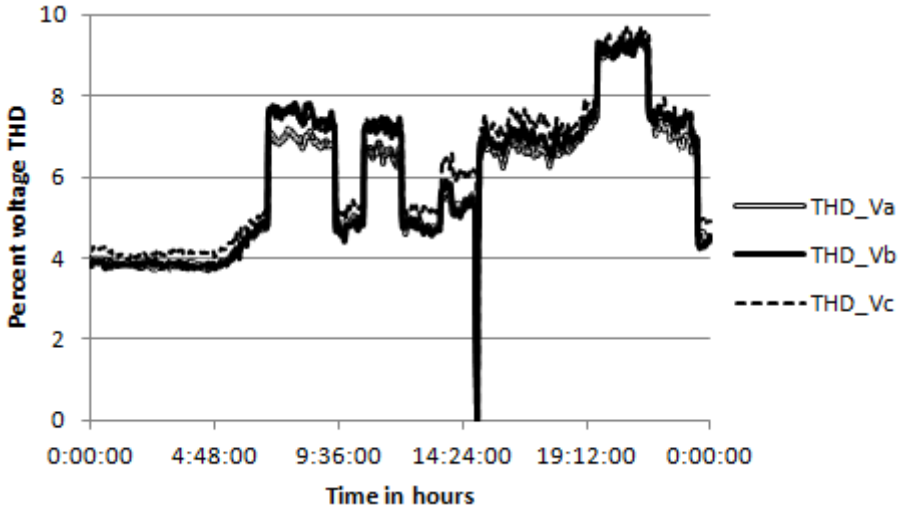

Figure 3.3 Variation in Voltage THD in All Three Phases at FeederDAS01

B. Individual harmonic current components in the feeder

Individual harmonic currents and voltages up to 15th harmonic are measured at all the feeder DAS locations. The measurements covering a span of one hour during the afternoon and night are available for a period of two days. Figure 3.4 and Figure 3.5 display the individual harmonic currents measured in the phase C at the feeder end from 12:00 P.M. to 1:00 P.M. and 12:00 A.M. to 1:00 A.M. on January 1, 2013. It is seen that the third harmonic current content is higher than rest of the harmonic spectral currents during both the periods and the harmonic current magnitude decreases with increase in the harmonic order. Further, the currents contributed by even harmonics are insignificant.

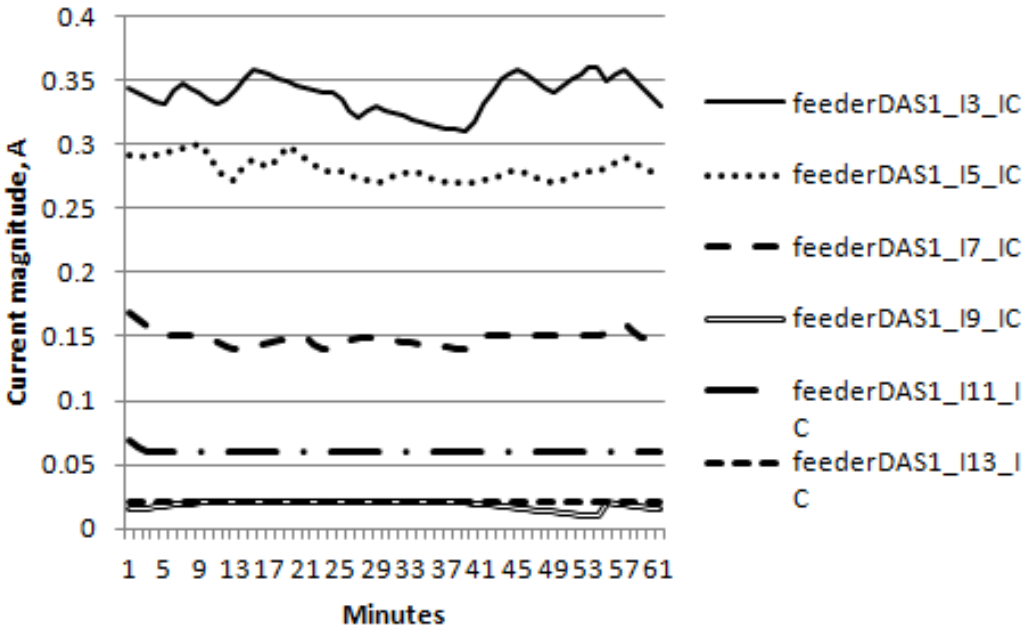

Figure 3.4 Individual Harmonic Currents Measured from 12:00 A.M.-1:00 A.M.

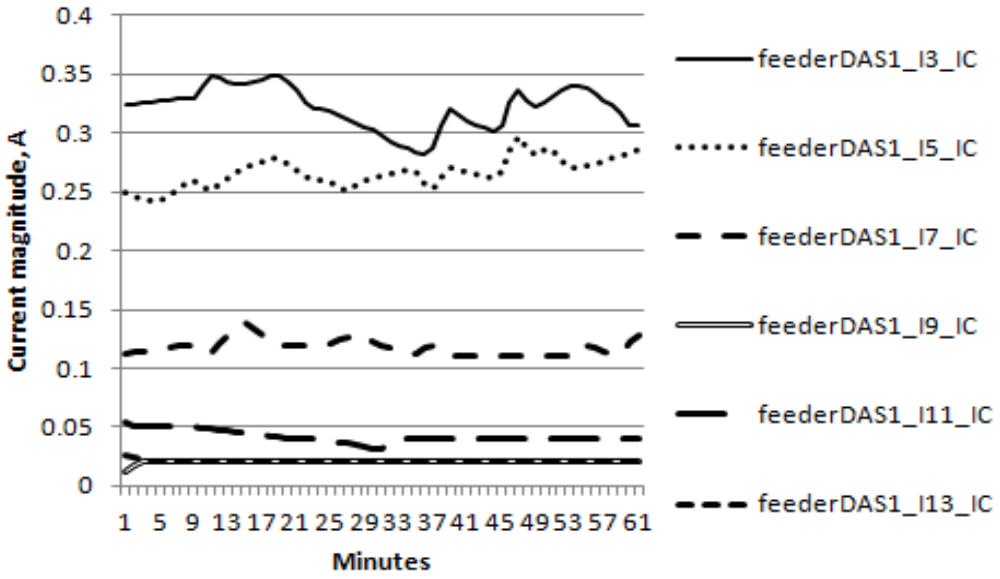

Figure 3.5 Individual Harmonic Currents Measured from 12:00 P.M.-1:00 P.M.

3.4 Harmonic Analysis in OpenDSS

The impact of non-linear loads on the voltage and current distortion is studied by performing harmonic analysis study on the test bed feeder in OpenDSS. The idea is, given the harmonic spectrum associated with all the non-linear loads, to run the harmonic power flow at each harmonic frequency separately and capture the harmonic voltages at all nodes in the system due to propagation of harmonic currents.

For the test bed feeder, harmonic currents injected by the customer loads are not monitored. However, it is known that the loads served by this feeder are mainly residential type. The non-linear electronic loads can be represented as single phase rectifiers. The amplitude of harmonic current components of a square wave rectifier is given by *1/h* where *h* is the harmonic number. Due to lack of measurements, this (*1/h* rule) is an assumption made for calculation of the load

harmonic spectral components. The phase angle of harmonic current components is taken as zero degrees. For the case study reported here, the focus is on harmonic spectral components at and below 13^{th} harmonic.

The study is performed for system operating conditions observed at 8:00 P.M. on September 25, 2012. The feeder details are summarized below:

- Total active power consumed by the loads = 3878.428 kW
- Total reactive power consumed by the loads = 1597.9 kVAr
- Total PV generation: No operation of PV systems
- Capacitor banks: All the three capacitor banks are switched on
- Substation voltage: 1.04 p.u.

The voltage THDs and current THDs are measured by the power quality meters installed at six feeder DAS locations. However, there are no measurements related to the harmonic spectral components present in the three phase primary for the period of study. If the individual harmonic measurements are available, the zone division method or random current injection method should be used to calculate the load harmonic spectrum accurately and perform harmonic analysis. The status of capacitor banks is derived from reactive power profile at feederDAS05. The 'spectrum' object is used to define the harmonic spectrum of load with input parameters as harmonic number, harmonic current magnitude expressed as a percentage of fundamental load current and phase angle.

The individual customer loads are accumulated and applied as a spot load at the secondary of distribution transformer. Starting with an initial estimate of

10% current THD contributed by the non-linear portion of accumulated load, the harmonic spectral components of the total load current are calculated by,

$$I_1.ITHD = I_3 * \sqrt{1 + \left(\frac{3}{5}\right)^2 + \left(\frac{3}{7}\right)^2 + \left(\frac{3}{9}\right)^2 + \left(\frac{3}{11}\right)^2 + \left(\frac{3}{13}\right)^2} \quad (3.3)$$

$$I_1.ITHD = I_5 * \sqrt{1 + \left(\frac{5}{3}\right)^2 + \left(\frac{5}{7}\right)^2 + \left(\frac{5}{9}\right)^2 + \left(\frac{5}{11}\right)^2 + \left(\frac{3}{13}\right)^2} \quad (3.4)$$

$$I_1.ITHD = I_7 * \sqrt{1 + \left(\frac{7}{3}\right)^2 + \left(\frac{7}{5}\right)^2 + \left(\frac{7}{9}\right)^2 + \left(\frac{7}{11}\right)^2 + \left(\frac{7}{13}\right)^2} \quad (3.5)$$

$$I_1.ITHD = I_9 * \sqrt{1 + \left(\frac{9}{3}\right)^2 + \left(\frac{9}{5}\right)^2 + \left(\frac{9}{7}\right)^2 + \left(\frac{9}{11}\right)^2 + \left(\frac{9}{13}\right)^2} \quad (3.6)$$

$$I_1.ITHD = I_{11} * \sqrt{1 + \left(\frac{11}{3}\right)^2 + \left(\frac{11}{5}\right)^2 + \left(\frac{11}{7}\right)^2 + \left(\frac{11}{9}\right)^2 + \left(\frac{11}{13}\right)^2} \quad (3.7)$$

$$I_1.ITHD = I_{13} * \sqrt{1 + \left(\frac{13}{3}\right)^2 + \left(\frac{13}{5}\right)^2 + \left(\frac{13}{7}\right)^2 + \left(\frac{13}{9}\right)^2 + \left(\frac{13}{11}\right)^2} \quad (3.8)$$

where *ITHD* is the current total harmonic distortion expressed as a percentage of fundamental current, I_1 is the fundamental load current, and I_3, I_5, I_7, I_9, I_{11}, I_{13} are harmonic currents present at harmonic orders of 3, 5, 7, 9, 11, 13 respectively. The harmonic solution mode is executed in OpenDSS and voltages and currents are recorded at each harmonic frequency using 'monitor' object. The results are exported to MS Excel, and voltage and current THDs are calculated. The above steps are continued until the calculated voltage THDs are within a good range of the measured voltage THDs. For the total harmonic distortion in load current of 6%, the calculated voltage THDs and currents THDs are compared with the measurements as shown in Table 3.2. The simulated voltages and currents at fundamental frequency are provided in Table 3.1.

Table 3.1 Steady State Power Flow Results

DAS location	Va (kV)	Vb (kV)	Vc (kV)	Ia (Amps)	Ib (Amps)	Ib (Amps)
feederDAS06						
Measured	7.458	7.439	7.431	132.13	119.27	118.93
Simulated	7.448	7.472	7.456	175.357	165.242	154.243
feederDAS05						
Measured	7.39	7.39	7.36	85.02	86.266	75.317
Simulated	7.364	7.438	7.459	86.1417	89.145	62.662
feederDAS03						
Measured	7.31	7.34	7.34	54.245	46.66	46.35
Simulated	7.28	7.369	7.459	49.202	45.7421	36.9906
feederDAS02						
Measured	7.3	7.29	7.31	30.522	29.403	14.47
Simulated	7.243	7.345	7.444	32.513	29.445	17.067
feederDAS01						
Measured	7.31	7.26	7.27	0.24	13.32	2.81
Simulated	7.212	7.282	7.429	0.5583	15.629	2.99

Table 3.2 Measured and Simulated Values of Voltage and Current THDs at Feeder DAS Locations

DAS location	THD_Va	THD_Vb	THD_Vc	THD_Ia	THD_Ib	THD_Ic
feederDAS06						
Measured	0.38	0.422	0.381	1.3	1.5	1.4
Simulated	1.28	1.08	1.24	6.15	6.28	6.26
feederDAS05						
Measured	4.07	3.9	4.22	11.95	9.82	12.37
Simulated	3.22	3.05	2.95	15.26	14.11	19.91
feederDAS03						
Measured	5.42	5.35	5.14	12.48	12.89	14.25
Simulated	5.07	4.83	4.66	16.9	17.16	21.78
feederDAS02						
Measured	5.75	5.72	5.69	14.35	15.01	14.95
Simulated	5.55	5.28	5.08	5.27	6.74	5.83
feederDAS01						
Measured	5.66	6.02	6.14	39.44	15.6	23.32
Simulated	5.65	5.48	5.16	6.66	7.25	4.78

Note that all the THDs are expressed as percentage of fundamental quantities.

It is observed from Table 3.2 that the simulated values of voltage THDs are quite close to the measured voltage THDs with the use of theoretical assumptions and calculations of load current injections. However, the current THD is overestimated at locations near head and middle of the feeder while underestimated at end of feeder. The fundamental currents at the end of feeder are very low. For the measured current THD of 39.44%, the fundamental current is 0.24 A. The individual load harmonics data is not available. Locating the harmonic sources is possible when harmonic content in branch currents is known and this can help in predicting the actual load current harmonics and their magnitudes.

To get a visual idea of voltage distortion along the feeder starting from substation till far end of the feeder, voltage total harmonic distortion (THD_V) is plotted for all three phases. Figure 3.6 shows the variation in voltage THD in all three phases plotted against the Y co-ordinate of buses in the test bed feeder.

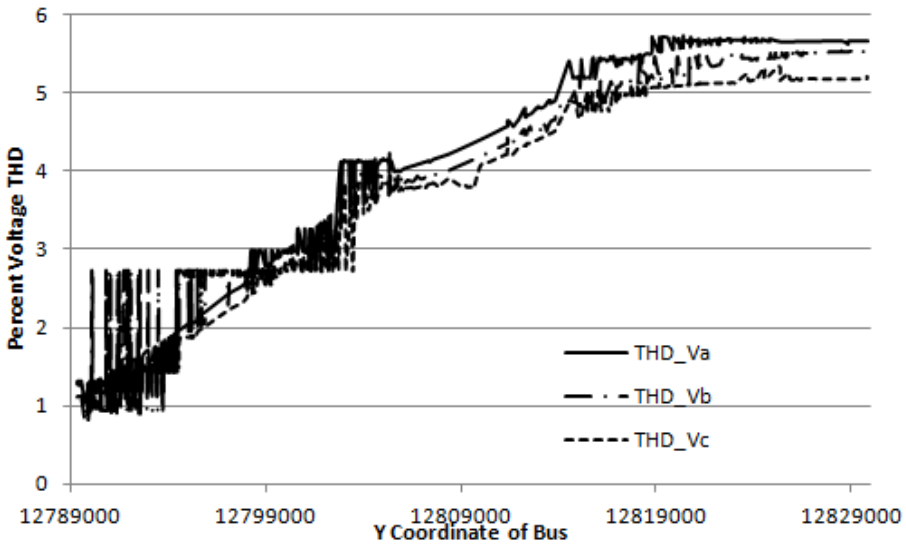

Figure 3.6 Variation in Voltage THD Starting from Substation Till the End of Feeder

The voltage THD is found to be minimum (around 1%) at the substation. It increases along the three phase primary as the distance from substation increases. Customers located in near proximity of substation are expected to experience distortion smaller than customers served downstream from far end of feeder. The customer loads generate currents rich in harmonic content and the harmonic currents travel along the feeder towards the substation source causing a voltage drop at each harmonic frequency. Thus, current distortion gives rise to voltage distortion due to the impedance offered by different feeder elements. The smaller source impedance at feeder head causes smaller distortion, and the impedance increases as various network components, like lines and transformers get added causing increase in voltage distortion at the far end of feeder. The end of the feeder experiences maximum voltage distortion of approximately 5.5%.

The load current harmonics are the cause of voltage distortion, but it should be noted that the load has no control over voltage distortion. The same load placed at two different locations in the system will result in two different voltage distortion values. This fact is recognized and serves as a basis for division of responsibilities for harmonic control that are recommended in IEEE 519 [20]:

- The control over the amount of harmonic current injected into the system takes place at the customer end connections.
- Assuming the harmonic current distortion is within the reasonable limits, control over harmonic voltage distortion is often a responsibility of the utility as voltage distortion depends on system impedance.

3.5 Frequency Scan Study

The objective of the frequency scan technique is to derive the frequency response of a network looking from a specific bus. One ampere current is injected into the bus at a frequency different than the fundamental frequency and the basic network equation, $YV=I$ is used to calculate the voltage or impedance response. The frequency is varied in discrete steps to cover a range of frequencies and the frequency scan technique can be used to identify potential resonant conditions, if any, related to the bus under consideration. The concept of using a 'frequency scan' is common in electric power quality studies because this approach gives a visual appreciation of the frequency response of a circuit.

The aforementioned technique can be best explained with an example. Consider the bus which serves a large load and has a large scale three phase PV system connected (P=400 kW) is selected for current injection. This bus is located at a distance of approximately 4 miles from the substation. The currents injected can be defined using phase or symmetrical components. For the test bed feeder under study, one ampere positive sequence or zero sequence current is injected and the frequency is increased above 60 Hz up to 2000 Hz in steps of 1 Hz. The response is captured at the bus with three phase capacitor bank installed, located close to the current injected bus. Since unit current is injected, the voltage at the bus of current injection would be equal to driving point impedance seen from that bus. One unit positive or zero sequence current injection at the bus of interest is used to derive the positive or zero sequence driving point network impedance seen from the same bus. The voltage response at any other bus close to the current

injected bus will be equal to the transfer impedance seen from that bus. Figure 3.7 and Figure 3.8 show the impedance response at the bus with capacitor bank for positive sequence and zero sequence current injection respectively.

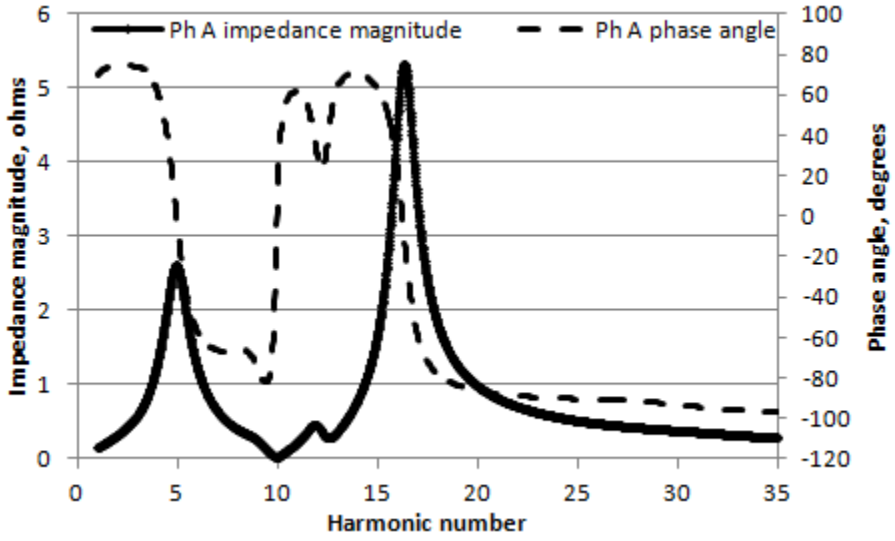

Figure 3.7 Positive Sequence Impedance Response at the Bus With Capacitor Bank

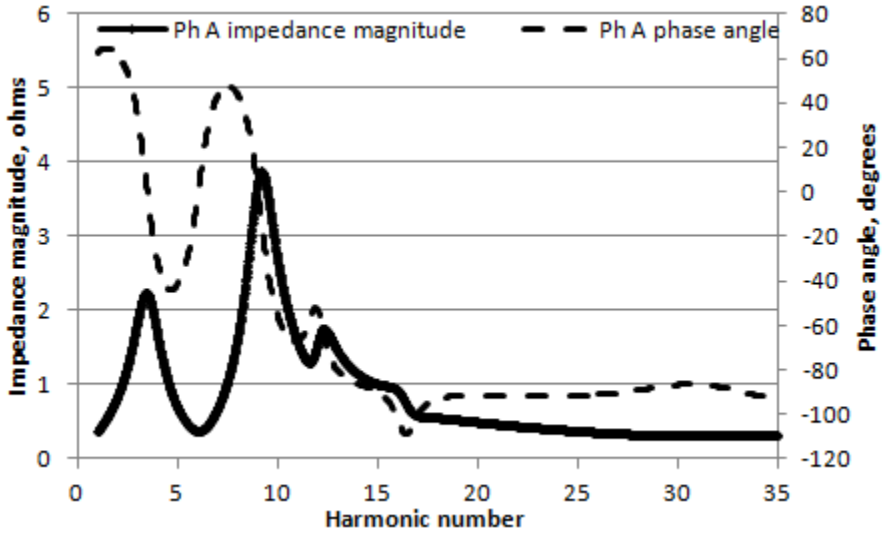

Figure 3.8 Zero Sequence Impedance Response at the Bus With Capacitor Bank

The two voltage controlled capacitor banks are then switched off and the impedance response is monitored at the three phase line closest to the capacitor bank location. Figure 3.9 and Figure 3.10 show the impedance response in phase A of the line for positive and zero sequence current injection respectively.

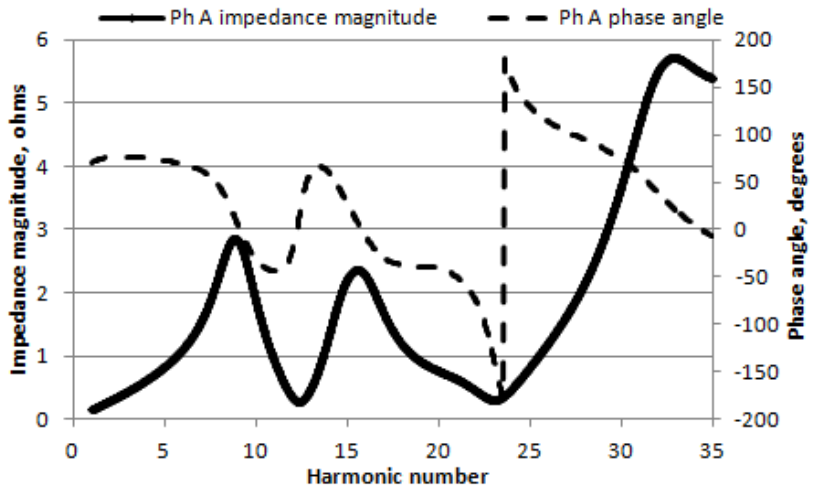

Figure 3.9 Positive Sequence Impedance Response at Line Close to the Capacitor Bank

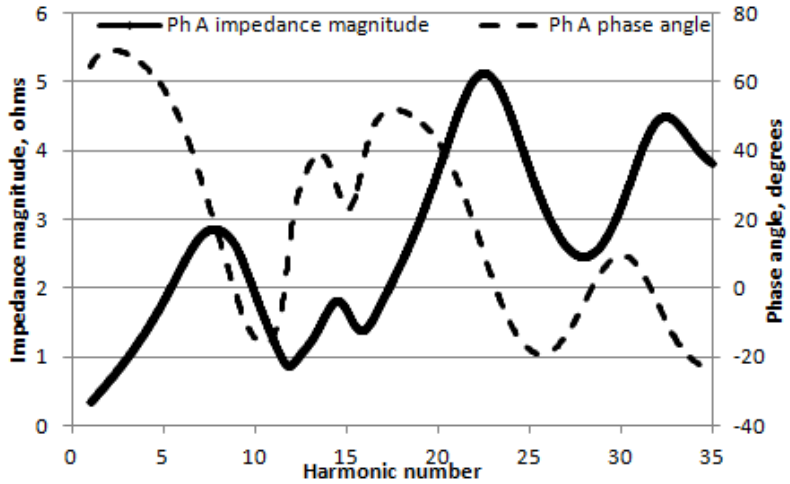

Figure 3.10 Zero Sequence Impedance Response at Line Close to the Capacitor Bank

The capacitor bank is located on the primary side of the test bed feeder and the voltage or impedance response is obtained for unit current injection. If the actual value of currents injected into the bus under study and the frequency of current injection are known, the voltages at the capacitor bank location can be calculated by multiplying with the scaling factor as the circuit is linear and scaling property applies to the linear circuits.

It should be noted that the frequency response is specific to the system operating conditions. The frequency response is influenced by shunt capacitor bank's operation (on or off), load variations, load damping, and variation in PV operation levels. The parallel and series resonances occurring in the network are identified by locating maxima and minima of impedance magnitude response, and in addition, the maxima and minima points should have phase angles crossing through 0^o or 180^o degrees. The resonant frequency has an inverse relationship with the kVAr rating of capacitor banks and it can be calculated based on system characteristics and ratings using,

$$h_r = \sqrt{\frac{MVA_{SC}}{MVAr_{cap}}} \tag{3.9}$$

where h_r is the harmonic at which resonance occurs, MVA_{SC} is the system short circuit MVA and $MVAr_{cap}$ is the rating of capacitor bank. It can be seen from the results that the first resonant peak shifts to a higher frequency when the two capacitor banks are switched off.

3.6 Summary

This chapter focuses on investigating the effect of distributed non-linear loads on the voltage and current distortion. Real measurements and harmonic analysis tool in OpenDSS are used to quantify the low order harmonics present in the test bed feeder using indices such as voltage and current THDs. Measurements and simulation results show the voltage distortion increases towards the end of feeder and a maximum voltage THD of 5-5.5% is calculated from the simulation results. The frequency scan technique is suggested to identify any potential resonant conditions or unacceptable levels of amplitudes of the low order harmonic spectral components. The frequency scan technique is used to study the frequency response at the bus located in the middle of feeder with and without capacitor banks.

CHAPTER 4

IMPACT OF PV RESOURCES ON POWER QUALITY OF THE TEST BED FEEDER

4.1 The Inverter Interface for PV Systems

PV systems are connected to the grid through inverters, which convert DC power generated by PV panels to AC power. The inverter configuration and design plays an important role in ensuring a safe and reliable grid connection of the PV system. Due to the advances in the manufacturing technologies of semiconductor devices, high speed switching devices are used with various PWM techniques to provide efficient DC-AC conversion with high power factor and low harmonic distortion. The different topologies of grid-connected PV inverters are summarized below [17] [47]:

- A single stage inverter forms a centralized structure and performs all the functions such as maximum power point tracking (MPPT), current control, and inversion. Earlier, the single stage inverters were line commutated by means of thyristors with poor power quality [17]. Modern central inverters use IGBTs and are self-commutated with improved power quality.
- Currently, string inverters are widely used in which a single string of PV modules is connected to the inverter. A separate DC-DC converter is employed for MPPT and voltage amplification, if required, and a DC-AC inverter controls the grid current by means of PWM or bang-bang operation. In cases where nominal power is high, it is wise to operate the inverter in

PWM mode. IGBTs and MOSFETs are commonly used for switching purposes. According to the International Energy Agency (IEA) survey, about 38% of inverters, rated less than 50 kW, use MOSFETs with switching frequencies in the range of 10-20 kHz, and 62% of inverters use IGBTs with a switching frequency of 20 kHz [47].

- Multi-string inverters are developed from the basic string inverter. In this topology, every PV string has a separate DC-DC converter which is then connected to a common DC-AC inverter for power inversion. The advantage of multi-string inverter is that each PV string can be controlled individually.

The selection between different topologies depends on various factors such as weight, cost, power conversion efficiency, size, and power quality. Depending on the electrical isolation between the PV panel and utility grid, the inverter can be isolated or non-isolated. The galvanic isolation is provided by means of a transformer, which has an influence on the PV system's efficiency. Some inverter designs use transformerless topologies.

4.2 PWM Inverters

The single phase PV systems deployed on the test bed feeder employ self-commutated PWM inverters. In the SPWM technique, in order to obtain a sinusoidal voltage waveform with desired amplitude and frequency at the inverter output, a sinusoidal reference signal is compared with a triangular carrier waveform. The reference signal is used to modulate the switch duty ratio and has frequency

equal to the frequency desired at the inverter output voltage. The frequency of the triangular carrier waveform defines the inverter switching frequency. The amplitude modulation ratio, m_a and frequency modulation ratio, m_f is given by,

$$m_a = \frac{V_{ref}}{V_{tri}} \tag{4.1}$$

$$m_f = \frac{f_s}{f_1} \tag{4.2}$$

where V_{ref} is peak amplitude of the reference signal, V_{tri} is peak amplitude of the triangular carrier signal, f_s is the carrier frequency (or inverter switching frequency), and f_1 is the desired fundamental frequency.

A. PWM with bipolar switching design

The single phase full-bridge inverter is shown in Figure 4.1. In the bipolar switching design, diagonally opposite switches from the two legs of the full-bridge inverter switch on and off simultaneously and output terminal voltage of inverter switches between $+V_d$ and $-V_d$ where V_d is the DC input voltage of inverter. The high frequency spectral components present in the inverter output voltage consists of sidebands centered on the switching frequency, f_s and its multiples, $2f_s$, $3f_s$.

B. PWM with unipolar switching design

In this design, the two legs of the full-bridge inverter are controlled separately and the switches in the two legs are not switched simultaneously as in the bipolar design. The output voltage of the inverter switches between 0 and $+V_d$ or 0 and $-V_d$. The dominant frequency above the 'power frequency' (i.e., 60 Hz) is

twice the switching frequency and high frequency spectral components include sidebands centered at $2f_s$, $4f_s$,….The high frequency spectral content for unipolar switching design is lower as compared to the bipolar design.

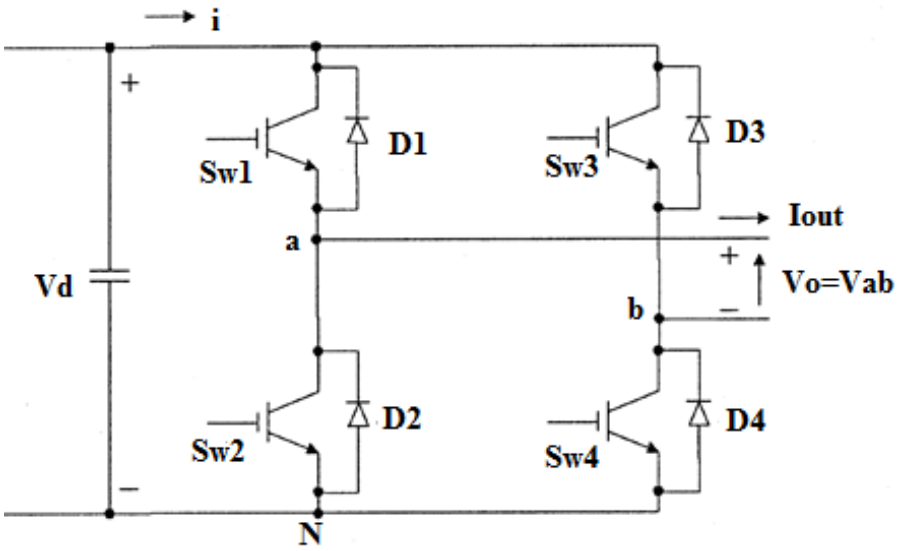

Figure 4.1 Single Phase Full-Bridge Inverter

A three phase inverter can be designed by combining three single phase full-bridge inverters. A more complete discussion of the spectrum of PWM voltages appears in [18], [48].

C. Determining the frequency spectrum of a PWM signal

The frequency spectrum of a PWM signal is generally obtained by application of fast Fourier transform (FFT) on a digitally simulated switched waveform. However, the accuracy of this technique is limited by number of samples and is affected when the carrier-to-fundamental frequency ratio is large and represents a non-integer value [49]. The accuracy also depends on the computational capabilities of simulation tool. A theoretical approach to determine the harmonic

content in a PWM signal is based on applying double Fourier series expansion in two variables and the approach is discussed in detail in [50], [51]. The double Fourier series method calculates the coefficients of DC offset, fundamental frequency and baseband harmonic components, high frequency components related to the carrier frequency, and sideband harmonics around the carrier frequency components present in the PWM spectrum. The sideband harmonics components present around the carrier frequency and their amplitudes are influenced by the nature of sinusoidal modulating waveform (with or without low harmonic components) and selection of modulation strategy. The other factors which influence the frequency spectral components of the modulated signal include design parameters such as overmodulation and undermodulation, small or large value of frequency modulation. Nowadays, multi-level PWM inverters are designed to reduce the harmonic distortion in the output voltage waveform. The accurate determination of inverter output voltage spectrum thus depends on the consideration of various design parameters mentioned above.

4.3 Details of the PV Systems Installed on the Test Bed Feeder

For the study purpose, single phase PV inverters deployed on the feeder are grouped into two categories based on the inverter manufacturers, namely group A and group B. The ratings of the small scale residential PV systems vary between 2 and 4 kW. The large scale three phase PV system rated at 700 kW is referred to as 'PVsystem1'. The other three phase PV system rated at 400 kW will be called 'PVsystem2' henceforth in the text.

A. Topology of the PV inverters

Most of the single phase PV inverters on the test bed feeder use H-bridge topology with unipolar PWM switching design. This is a commonly used design; advantages being improvement in quality of current injected in the grid, and less electromagnetic interference. Another popular inverter topology is a hybrid H-bridge design. The hybrid H-bridge consists of a standard H-bridge topology combined with asymmetric unipolar modulation. In this design, one of the legs of the asymmetric H-bridge is switched at a low frequency (60 Hz), and the other leg is PWM modulated to give a sinusoidal output voltage. The high frequency spectral components present in the inverter output voltage are similar to that observed in the bipolar design.

B. Frequency spectrum of the PV systems

The inverter manufacturers provide details regarding the electrical characteristics of the PV systems and compliances with different IEEE standards in the inverter data sheet. The total distortion of the current, given by THD, is normalized by the rated fundamental current and is specified to be 3% in most of the inverters. Assuming the background supply voltage is not distorted and the PV controller design has no deficiency, the PV system will generate only high frequency current spectral components due to the electronic switching techniques.

The measurements related to high frequency spectral components are not available on the test bed feeder. The power quality meters installed on the test bed feeder have limited bandwidth and are not capable of recording any high frequency components. Further, the calculation of frequency spectral components based

on theoretical analysis is very complex and with various inverter design parameters being unknown, it is difficult to incorporate this analysis in the study.

C. Approach for the high frequency power flow study

It is known that the high frequency spectral components generated by the PV inverter depend on the inverter switching frequency and the modulation strategy. The switching frequencies of some of the PV inverters installed on the test bed feeder are found from the inverter model data. Most inverter manufacturers do not specify the inverter switching frequency, but examination of typical designs indicates that a suitable frequency range for the study is 2–20 kHz. For the study, only the first dominant high frequency, present above the fundamental frequency, is considered and current THD is used to define the magnitude of the spectral current component at the dominant frequency. The spectral current components occurring at frequencies above the first dominant frequency are ignored due to their low and decaying magnitudes. The frequencies of current injection according to the inverter manufacturers are provided below:

- Group A - 12 kHz
- Group B - 16 kHz
- PVsystem1 - 10 kHz
- PVsystem2 - 18 kHz.

The magnitude of the high frequency spectral current component remains same for all the operating levels of PV output power. The spectral current component magnitude occurring at first dominant frequency will be 3% of the funda-

mental current when PV inverter is operated at rated power output. The calculation is based on the specified current THD and frequency spectrum approximation. For PV system operating at different power output level (below the rated power output), the magnitude of high frequency spectral component expressed as a percentage of fundamental current will increase and is calculated using the relation given in Figure 4.2. The phase angle of the high frequency spectral currents generated by distributed PV is random in nature with no relation to the phase angle of fundamental component.

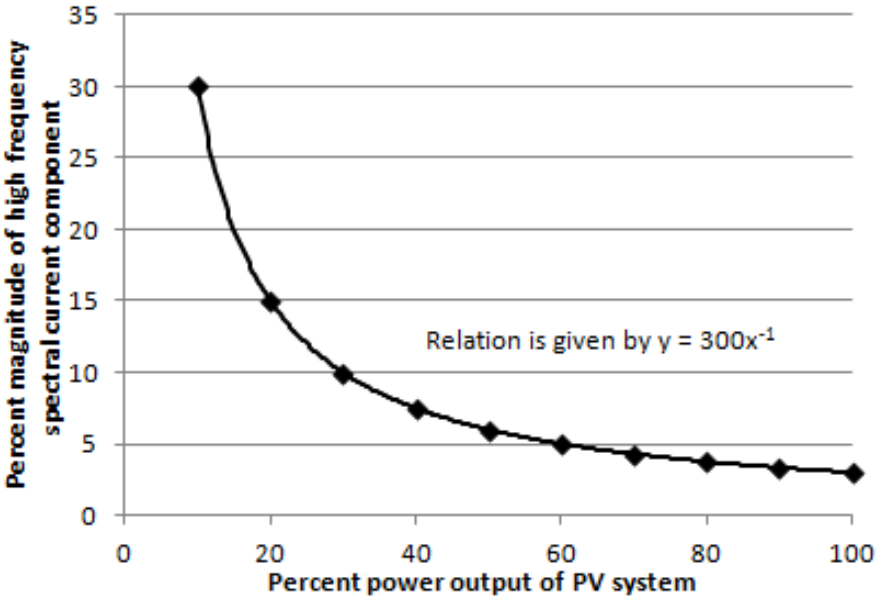

Figure 4.2 Percent Magnitude of High Frequency Spectral Current Component for Different Operating Levels of PV System

4.4 High Frequency Power Flow Simulations and Results

The impact of high frequency spectral currents on power quality of the test bed feeder is studied for high PV penetration. The highest PV penetration case is observed on September 25, 2012 at 12:44 P.M. The summary of system operating conditions corresponding to this period is given in Table 4.1.

Table 4.1 Total Load and PV Generation in the Test Bed Feeder

	Active power, kW	Reactive power, kVAr
Total load	2884.443	1609.544
Total PV generation	1266.9	0

For the study, two cases are considered to analyze the effect of different levels of PV penetration.

A. Case I: PV systems operating at their ratings

All the system operating conditions observed for highest PV penetration case are kept same and PV systems are now operated at their ratings. The total PV generation accounts for 1.56 MW. The 'Isource' object in OpenDSS is used to inject the high frequency spectral current components in the feeder. The magnitude of the spectral current component is determined from Figure 4.1 and the phase angle is taken as zero degrees for the initial analysis. The PV systems are modeled as negative loads and the harmonic spectrum associated with load elements are edited to include only fundamental component and no harmonic or high frequency components.

The substation voltage at the time of snapshot simulation is 1.04 p.u. and it is modeled as a balanced three phase voltage source. Initially, all the capacitor banks are switched on and power flow is run in OpenDSS. The voltage profile is found to improve along the feeder due to the presence of capacitor banks and the PV is capable of improving voltage locally. The capacitor bank control algorithm defined in OpenDSS turns off the capacitor bank located in the middle of the three phase lateral. The resulting voltage profile along the feeder length is shown in Figure 4.3.

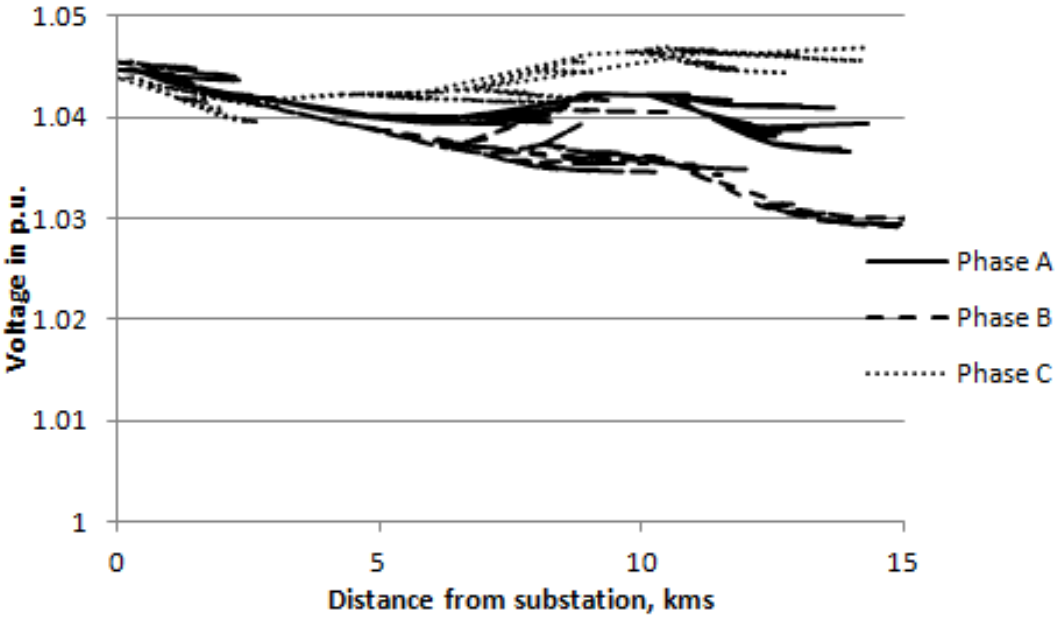

Figure 4.3 Voltage Profile Along the Test Bed Feeder

The harmonic mode is then executed in OpenDSS to give voltages and currents in all the feeder elements at each of the frequency defined in the circuit. The 'monitor' objects are placed at the feeder DAS locations. The general

MATLAB code for high frequency power flow study is provided in Appendix A. The voltage THDs and current THDs are calculated and shown in Table 4.2. The THDs are calculated taking into account only the high frequency components and are expressed as a percentage of fundamental components.

Table 4.2 Voltage and Current THDs at Feeder DAS Locations

Location	Vthd_phA	Vthd_phB	Vthd_phC	Ithd_phA	Ithd_phB	Ithd_phC
DAS06	0.017	0.021	0.022	0.058	0.076	0.068
DAS05	0.350	0.462	0.186	5.717	2.240	0.457
DAS04	0.564	0.391	0.085	7.960	2.319	0.687
DAS03	0.499	0.409	0.415	3.752	3.437	3.009
DAS02	0.067	0.115	0.145	0.092	0.182	1.504
DAS01	0.043	0.035	0.015	4.306	0.373	3.556

Note that all the THD values are percentage values.

Another index studied is the distortion factor (DF) which gives the individual voltage distortion as,

$$DF = \frac{V_{high-frequency}}{V_{fundamental}} * 100 \tag{4.3}$$

The individual voltage distortion is calculated at all the system voltage levels and buses (7.2 kV, 120V and 277V). The maximum individual voltage distortion calculated as a percentage of the fundamental voltage and the bus number where it occurs is provided in Table 4.3.

The individual voltage distortion is found to be highest only at the buses that have PV systems connected. Also, these highest voltage distortion locations are found at the end of the single phase laterals where the system becomes weaker. For example, consider spectral current injections at 12 kHz (or 16 kHz) by

group A (or group B) inverters. The maximum individual voltage distortion is recorded at the node where group A PV inverter (or group B) is connected to the feeder. For the three phase PV system (referred as 'PVsystem1') injecting currents at 10 kHz, the maximum voltage distortion is experienced at single phase laterals and three phase primary nodes close to the PVsystem1. For the three phase PV system (referred as 'PVsystem2') injecting currents at 18 kHz, the bus where the PVsystem2 is connected (bus #2956) experiences maximum voltage distortion of approximately 3% while for the rest of system buses, the individual voltage distortion is less than 0.8%. The maximum individual voltage distortion is observed to be lowest for current injections at 10 kHz and for the remaining frequencies (12, 16, and 18 kHz), the maximum individual voltage distortion is in the range of 2%-3.5%.

Table 4.3 Maximum Individual Voltage Distortion at All the High Frequencies

Frequency	Maximum voltage distortion ph A	Maximum voltage distortion ph B	Maximum voltage distortion ph C
10 kHz	0.901% (67.522/7491.95) @ 1438	0.858% (64.06/7462.41) @1899	0.749% (0.94/125.38) @3764
12 kHz	2.097% (2.62/124.79) @3714	2.677% (3.332/124.46) @3046	1.59% (1.995/125.12) @2886
16 kHz	2.39% (2.99/124.97) @3304	1.665% (2.069/124.28) @3934	2.40% (3.014/125.38) @2336
18 kHz	3.31% (9.498/286.454) @2956	2.96% (8.535/288.11) @2956	3.15% (9.094/288.29) @2956

'Format of the results shown in Table 4.3: Percentage individual distortion (Voltage at high frequency / Voltage at fundamental frequency) @ system node number'

B. Case II: Doubling the PV generation at all the PV sites based on their ratings

The total PV generation in the test bed feeder accounts for 3.125 MW. The system load level and other operating conditions are kept same. The snapshot power flow is run in OpenDSS and the resulting voltage profile along the feeder length is shown in Figure 4.4. The two voltage controlled capacitor banks along the feeder are switched off by the capacitor control algorithm.

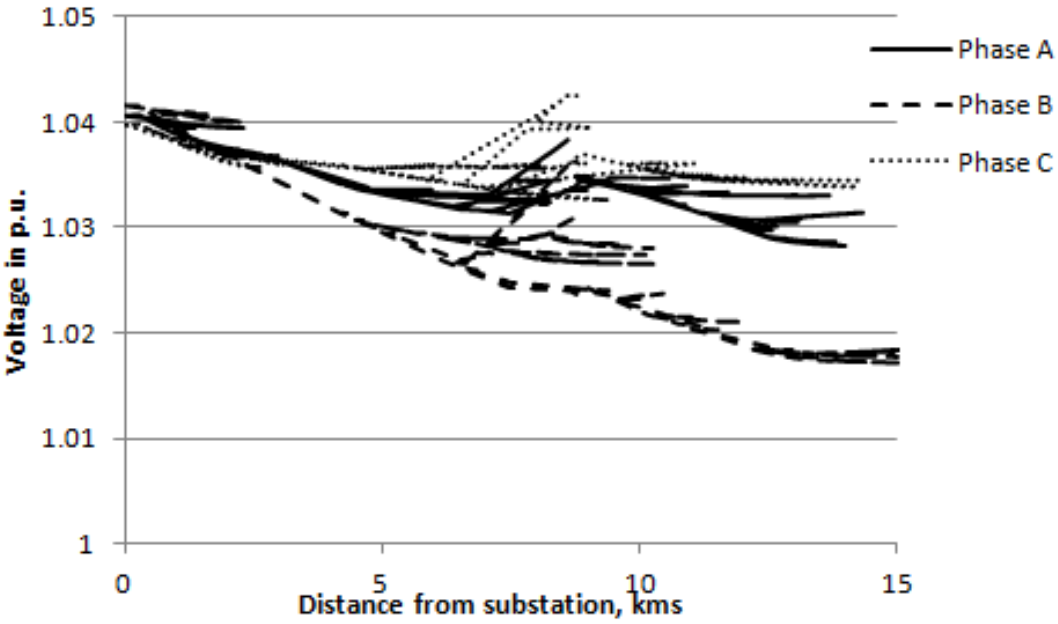

Figure 4.4 Voltage Profile Along the Test Bed Feeder

The harmonic mode is executed and the calculated voltage THDs and current THDs at the feeder DAS locations are shown in Table 4.4. The maximum individual voltage distortion in all three phases is shown in Table 4.5.

Table 4.4 Voltage and Current THDs at Feeder DAS Locations

Location	Vthd_phA	Vthd_phB	Vthd_phC	Ithd_phA	Ithd_phB	Ithd_phC
DAS06	0.0391	0.0638	0.0546	0.0928	0.2698	0.1812
DAS05	0.8420	1.4644	0.4120	2.5652	1.1082	0.0642
DAS04	1.4563	1.2076	0.1725	8.4218	2.9997	0.7795
DAS03	0.8864	1.5045	0.5811	9.4014	10.3597	2.7688
DAS02	0.3305	0.6930	0.6636	5.3763	2.4383	18.6619
DAS01	0.1460	0.0592	0.1812	10.9040	1.4394	36.2924

Note that all the THD values are percentage values.

Table 4.5 Maximum Individual Voltage Distortion at All the High Frequencies

Frequency	Maximum voltage distortion phA	Maximum voltage distortion phB	Maximum voltage distortion phC
10 kHz	2.13% (158.703/7448.27) @1438	1.98% (145.978/7381.8) @ 162	1.63% (122.128/7471.36) @ 1899
12 kHz	3.03% (3.759/123.96) @ 3714	3.5% (4.327/123.475) @ 3046	2.17% (2.689/124.16) @3782
16 kHz	3.187% (3.939/123.60) @3304	3.03% (3.669/121.01) @ 3846	3.24% (4.036/124.56) @2336
18 kHz	3.075% (8.77/285.07) @ 2956	2.91% (8.329/286.10) @ 2956	2.95% (8.528/288.24) @ 2956

i. Frequency scan for zero sequence current injection at PVsystem1 bus

A current source is modeled to inject one ampere zero sequence currents into the bus where PVsystem1 is connected and the frequency is increased in the steps of 1 Hz from 8 kHz to 11 kHz. The phase A impedance response observed from the same bus is shown in Figure 4.5. The phase A impedance magnitude is approximately 35 ohms for 1 A current injected at 10 kHz. Further, the frequency response for phases B and C do not show any high magnitudes of impedances

near 10 kHz. If the actual magnitudes of zero sequence currents are known, the voltages can be easily determined using linear scaling technique.

ii. Frequency scan for positive sequence current injection at PVsystem1 bus

A current source is modeled to inject one ampere positive sequence currents into the bus where PVsystem1 is connected and the frequency is increased in the steps of 1 Hz from 8 kHz to 11 kHz. The phase A impedance response observed from the same bus is shown in Figure 4.6. The impedance magnitude is around 12 ohms at 10 kHz, which is lower than the previous case. Also, the frequency response for phases B and C do not show any high magnitudes of impedances near 10 kHz.

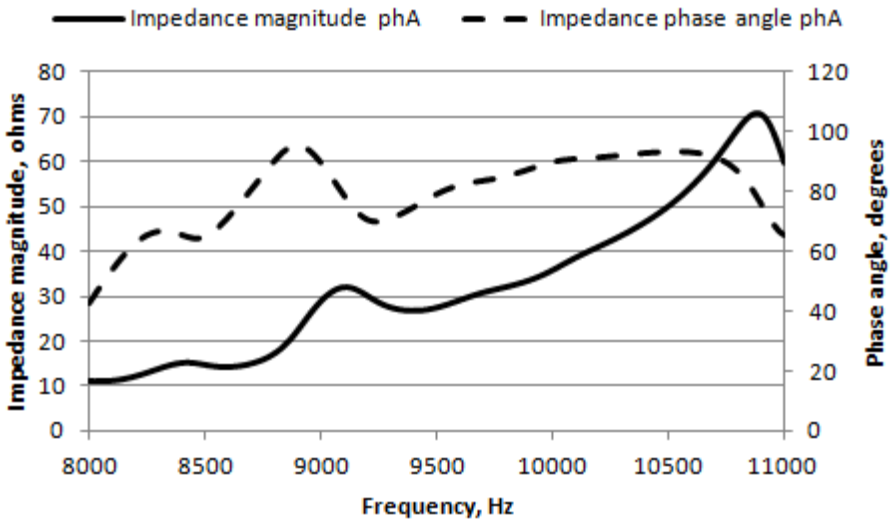

Figure 4.5 Impedance Magnitude and Phase Angle Response for Zero Sequence Current Injection

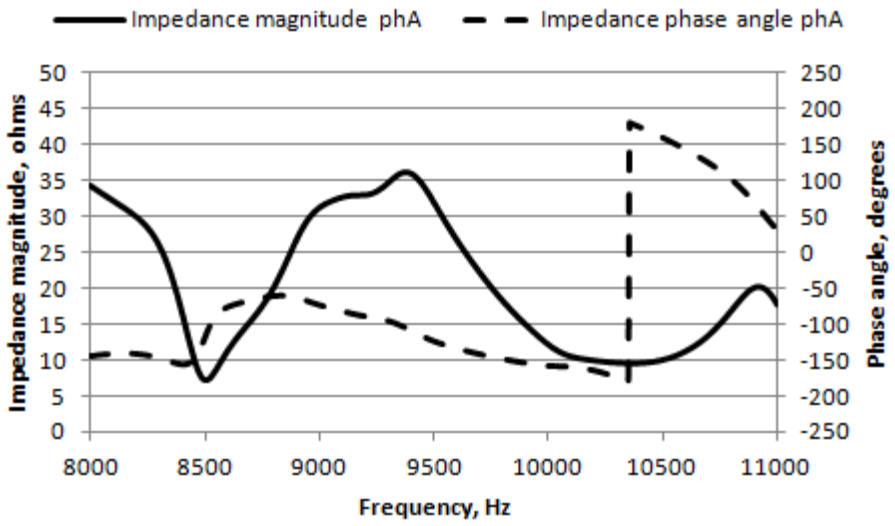

Figure 4.6 Impedance Magnitude and Phase Angle Response for Positive Sequence Current Injection

4.5 Analysis

The following analysis can be made based on the results for case I and II:

- With increase in the PV penetration level, the amount of spectral current injections increases and the total distortion in voltages and currents rises in the test bed feeder. The current THD is observed to be high at feeder DAS03 and it is majorly influenced by the spectral currents injections from the large scale three phase PV system, 'PVsystem1' located close to the DAS03 location. The current THD at feeder DAS01 is high (36% in phase C) but the fundamental currents at DAS01 location have very low values, less than 1 A (0.7 A in phase C).
- The maximum individual voltage distortion increases with an increase in PV generation for the frequencies of 10 kHz, 12 kHz and 16 kHz as ex-

pected. However, at 18 kHz, the maximum individual voltage distortion decreases by a very small amount. The slight decrease in the high frequency phase voltages observed in case II at 18 kHz is due to the additional load damping modeled at the bus with PVsystem2. As a result, the high frequency spectral current components injected into the feeder reduce, resulting in slightly lower voltage distortion at 18 kHz.

- In cases I and II, all the single phase distributed PVs are set to inject spectral currents with a phase angle of zero degrees. This is an assumption made for the initial assessment and worst case scenario analysis. However, this assumption of phase angle might not represent the real case scenario. To analyze the effect of random phase angles on high frequency voltages and individual voltage distortion, the phase angles of spectral currents injected by single phase distributed PVs are randomly varied for case II. The random number generator in MATLAB is used to generate the phase angles and results for two different trials using random phase angles are presented. Table 4.6 shows the maximum individual voltage distortion for current injections with random phase angles at 12 kHz for two different trials. Table 4.7 shows the maximum individual voltage distortion for currents injections with random phase angles at 16 kHz for two different trials. It is found that changing the phase angles of high frequency spectral currents affects the high frequency voltages, decreases the maximum individual voltage distortion as compared to the case where all the high fre-

quency injection currents are in phase, and also influences the location where highest distortion is observed.

Table 4.6 Maximum Individual Voltage Distortion for Current Injections With Random Phase Angles at 12 kHz

Trial number	Maximum voltage distortion phA	Bus number phA	Maximum voltage distortion phB	Bus number phB	Maximum voltage distortion phC	Bus number phC
1	2.02%	3306	3.09%	3046	2.15%	3764
2	2.18%	2576	2.19%	3938	2.16%	3782

Table 4.7 Maximum Individual Voltage Distortion for Current Injections With Random Phase Angles at 16 kHz

Trial number	Maximum voltage distortion phA	Bus number phA	Maximum voltage distortion phB	Bus number phB	Maximum voltage distortion phC	Bus number phC
1	3.12%	3304	2.66%	2200	3.11%	2336
2	2.58%	2510	2.65%	3560	2.63%	2398

CHAPTER 5

CONCLUSIONS AND FUTURE WORK

5.1 General Conclusions

The work presented in this thesis concentrates on power quality assessment of a real operational distribution feeder. The main concern is investigation of harmonic and high frequency spectral voltages and currents in the test bed feeder. The effect of non-linear loads and PV resources on spectral distortion in voltages and currents is studied separately. The various harmonic studies performed on the test bed feeder along with the general conclusions are summarized below:

- The modeling of the test bed feeder is accomplished for two different ranges of frequencies, one considering the low order baseband harmonics at and below 13th harmonic (780 Hz), and the other covers frequencies in the range of 2-20 kHz. A full three phase representation of the feeder is used in OpenDSS and the details about modeling of various feeder components based on the frequency of interest are presented in Chapter 2.
- Based on the field data and individual harmonics measurements, the test bed feeder is validated using two techniques, zone division method and random current injection method. The zone division method is based on applying the measured harmonic currents magnitudes at feeder DAS locations to replicate the system behavior at each harmonic frequency and the simulation results are found to match well with the measured harmonic

voltages for the 3rd and 5th harmonic at feeder DAS locations. The random dispersion of phase angles of individual load current harmonics for harmonics of order 7 and above is incorporated in the random current injection technique. The feeder validation method helps confirming the accuracy and reliability of the test bed feeder model. There are no measurements available related to the high frequency components in test bed feeder. Hence, the feeder model is assumed to be accurate for high frequency studies once it is validated for low order harmonics.

- The effect of distributed non-linear loads on voltage and current distortion can be quantified using voltage and current THD, and this has been discussed in Chapter 3. The voltage THD profile along the test bed feeder shows maximum voltage distortion is experienced at the end of feeder where the network becomes weak. The cases studied show maximum voltage THD of 5-5.6%. The frequency scan technique is adopted to study the frequency response of the network and identify the potential resonance conditions, if any, for a particular system operating conditions.
- The high frequency spectral currents injected by residential and large scale PV resources are studied in Chapter 4. High frequency power flow study shows that the total voltage and current distortion in the test bed feeder increases with an increase in the PV penetration level. The individual voltage distortion factor helps to identify if any of the high frequency injections are problematic and may result in high amplitudes of voltages in the

feeder. The high frequency voltages reported for the case studies do not show any values large enough to be a concern. The maximum individual voltage distortion is in the range of 3-3.5% (considering all the high frequencies of interest) for the worst case scenario.

- Simulation results from high frequency power flow study show that the maximum individual voltage distortion is seen at the buses which are connected to PV systems and are located at the end of feeder laterals. The phase angles of high frequency spectral currents generated by PV resources are random and asynchronous to the fundamental frequency components. Changing the phase angles of spectral currents affects the high frequency phase voltage magnitudes, and reduces the maximum individual voltage distortion as compared to the case where all the high frequency injection currents are in phase (i.e., phase angle of zero degrees). This is illustrated for current injections by the single phase PV systems distributed throughout the test bed feeder.

5.2 Future Work

There is a growing interest in analyzing the high frequency spectral voltage and current components present in the feeder due to PV resources. Some of the areas which can be explored for further studies are:

- Developing the monitoring infrastructure to measure the high frequency voltages and currents in the feeder will help in benchmarking the high frequency model representation of feeder. Calculation of frequency spectrum

of a PWM signal is very complex and detailed information regarding inverter design, modulation strategy, and design parameters must be gathered to accurately determine the frequency spectrum of inverter output voltage or current.

- The PV systems are modeled as negative loads with unity power factor in the study. The capability of PV inverters to provide reactive power and actively regulate the voltage should be incorporated in future studies.
- The loads are modeled as constant *PQ* in the present study. In future studies, different load models such as constant impedance, constant current, and ZIP models should be incorporated based on the knowledge on the customer load types and their composition. Identification of loads served by the feeder secondaries will help in accurate determination of aggregate harmonic load model. In Norton equivalent load model, the shunt admittance branch represents linear load at the point of common coupling (PCC) and should be modeled based on the load data.
- The individual voltage and current harmonic measurements at PCC can be used to develop correlation based techniques to identify the individual harmonic impact of multiple non-linear loads in the system [52]. Another method to study the harmonic impact of non-linear loads suggests building an equivalent circuit model to separate harmonic contribution of a customer from the utility system at PCC [53]. The harmonic measurements at PCC provide a valuable data for calculation of harmonic impedance.

While the aforementioned techniques help in quantifying the load harmonic impacts, identifying the main harmonic sources is an important task in power quality assessment and should be explored in future studies [54]. The various methods for identification of harmonic sources and assessing the harmonic impacts of multiple loads are mentioned in [55]. These methods should be reviewed, studied and incorporated in the future work if measurements are available.

REFERENCES

[1] U.S. Department of Energy, "2012 Renewable energy data book," DOE/GO-102013-4291, October 2013.

[2] U.S. Department of Energy, "2010 Solar technologies market report," available online at: http://www.nrel.gov/docs/fy12osti/51847.pdf.

[3] U.S. Energy Information Administration, "Short term energy outlook," http://www.eia.gov/forecasts/steo/pdf/steo_full.pdf, September 2012.

[4] U.S. Department of Energy, "The potential benefits of distributed generation and rate-related issues that may impede their expansion," available online at: http://www.ferc.gov/legal/fed-sta/exp-study.pdf.

[5] I. Waseem, M. Pipattanasomporn, and S. Rahman, "Reliability benefits of distributed generation as a backup source," presented at the IEEE Power Energy Soc. Gen. Meeting, Calgary, AB, Canada, 2009.

[6] R. E. Brown, "Reliability benefits of distributed generation on heavily loaded feeders," *Proc. of the IEEE/PES General Meeting*, pp. 1-4, Jul. 2007.

[7] G. Jobs, B.-T. Ooi, D. McGillis, F.D. Galiana, and R. Marceau, "The potential of distributed generation to provide ancillary services," in *Proc. IEEE Power Engineering Society Summer Meeting, 2000*, vol. 3, pp. 1762-1767.

[8] P. A. Daly, J. Morrison, "Understanding the potential benefits of distributed generation on power delivery systems," *Rural Electric Power Conference*, pp. A201-A213, 2001.

[9] R. A. Walling, R. Saint, R. C. Dugan, J. Burke, L. A. Kojovik, "Summary of distributed resources impact on power delivery systems," *IEEE Trans. on Power Delivery*, vol. 23, no. 3, pp. 1636 – 1644, July 2004.

[10] P. Mitra, G. T. Heydt, V. Vittal, "The impact of distributed photovoltaic generation on residential distribution systems," *in Proc. North American Power Symposium*, Urbana IL, pp. 1-6, Sept. 2012.

[11] T. Ackermann, V. Knyazkin, "Interaction between distributed generation and the distribution network: operation aspects," *Transmission and Distribution Conference and Exhibition 2002: Asia Pacific. IEEE/PES*, vol. 2, pp. 1357-1362, 6-10 Oct. 2002.

[12] A. Girgis, S. Brahma, "Effect of distributed generation on protective device coordination in distribution system," *in Proc. Large Engineering Systems Conf.*, Halifax NS, pp. 115-119, 2004.

[13] S. M. Brahma, A. Girgis, "Development of adaptive protection scheme for distribution systems with high penetration of distributed generation," *IEEE Transactions on Power Delivery*, vol. 19, no. 1, pp. 56-63, Jan. 2004.

[14] R. A. Walling, N. W. Miller, "Distributed generation islanding-implications on power system dynamic performance," *IEEE Power Engineering Society Summer Meeting*, vol. 1, pp. 92-96, 25 July 2002.

[15] V. Khadkikar, R. K. Varma, R. Seethapathy, A. Chandra, H. Zeineldin, "Impact of distributed generation penetration on grid current harmonics considering nonlinear loads," *3rd IEEE International Symposium on Power Electronics for Distributed Generation Systems (PEDG)*, pp. 608-614, 25-28 June 2012.

[16] IEEE standard for interconnecting distributed resources with electric power systems, IEEE Std. 1547-2003, pp. 1-16, 2003.

[17] S. B. Kjaer, J. K. Pedersen, F. Blaabjerg, "A review of single-phase grid-connected inverters for photovoltaic modules," *IEEE Transactions on Industry Applications*, vol. 41, no. 5, pp. 1292-1306, Sept.-Oct. 2005.

[18] Ned Mohan, Tore M. Undeland, William P. Robbins, *Power Electronics: Converters, Applications, and Design, Volume 1*, 3rd Edition: John Wiley and Sons, 2003.

[19] Electric Power Research Institute (January 1998): web-page available online at: http://www.epri.com/gg/newgen/disgen/index.html.

[20] J. Arrillaga , D. A. Bradley and P. S. Bodger, *Power system harmonics*, John Wiley and Sons, 1985.

[21] V. E. Wagner, J. C. Balda, D. C. Griffith, A. McEachern, T. M. Barnes, D. P. Hartmann, D. J. Pileggi, A. E. Emanuel, W. F Horton, W. E. Reid, R. J. Ferraro, W. T. Jewell, "Effects of harmonics on equipment," *IEEE Transactions on Power Delivery*, vol. 8, no. 2, pp. 672-680, Apr. 1993.

[22] Guide for harmonic control and reactive compensation of static power converters, IEEE Standard 519-1992, Piscataway, NJ.

[23] Yaosuo Xue, Liuchen Chang, Sren Baekhj Kjaer, J. Bordonau, T. Shimizu, "Topologies of single-phase inverters for small distributed power generators: an overview," *IEEE Transactions on Power Electronics*, vol. 19, no. 5, pp. 1305-1314, Sept. 2004.

[24] I. Holtz, "Pulsewidth modulation for electronic power conversion," in *Proc. of the IEEE*, vol. 82, no. 8, pp. 1194-1214, Aug. 1994.

[25] Xu, Wilsun, "Component modeling issues for power quality assessment," *IEEE Power Engineering Review*, vol. 21, no. 11, pp. 12-17, Nov. 2001.

[26] H. Akagi, H. Hasegawa, T. Doumoto, "Design and performance of a passive EMI filter for use with a voltage-source PWM inverter having sinusoidal output voltage and zero common-mode voltage," *Proceedings of IEEE PESC* , vol. 3, pp. 1543-1550, June 2002.

[27] L. Paulsson, B. Ekehov, S. Halen, T. Larsson, L. Palmqvist, A. Edris, D. Kidd, A J F Keri, B. Mehraban, "High-frequency impacts in a converter-based back-to-back tie; the eagle pass installation," *IEEE Transactions on Power Delivery*, vol. 18, no. 4, pp. 1410-1415, Oct. 2003.

[28] Inverters, converters, controllers and interconnection system equipment for use with distributed energy resources, UL 1741.

[29] H. W. Dommel, "*Electromagnetic transients program reference manual (EMTP Theory Book),*" Prepared for Bonneville Power Administration, Dept. of Electrical Engineering, University of British Columbia, Vancouver BC, Aug. 1986.

[30] G. Heydt, *Electric power quality*, Stars in a Circle Publications, Scottsdale, AZ, 1994.

[31] M. McGranaghan, R. C. Dugan, J. A. King, W. T. Jewell, "Distribution feeder harmonic study methodology," *IEEE Trans. on Power Apparatus and Systems*, vol. 103, no. 12, pp. 3663- 3670, 1984.

[32] IEEE Task Force on Harmonics Modeling and Simulation, "Modeling and simulation of the propagation of harmonics in electric power networks, Part 1 and 2," *IEEE Trans. on Power Delivery*, vol. 11, no. 1, pp. 452-474, January 1996.

[33] Carlos Gonzalez-Garcia and Jorge Pleite, "Transformer model in wide frequency bandwidth for power electronics systems," Hindawa Publishing Corporation, Advances in Power Electronics, Article ID 249146, vol. 2013.

[34] OpenDSS. [Online]. Available: http://sourceforge.net/apps/mediawiki/electricdss/index.php

[35] Roger C. Dugan, Thomas E. McDermott, "An open source platform for collaborating on smart grid research," *IEEE Power and Energy Society General Meeting*, 24-29 July 2011, pp. 1-7.

[36] R. Dugan, OpenDSS application workshop - Introduction, Electric Power Research Institute (EPRI), 2 Nov. 2009, Knoxville, TN.

[37] Roger C. Dugan, Mark F. McGranaghan, H. Wayne Beaty, *Electrical power systems quality*, New York: McGraw Hill, 1996.

[38] H. Sharma, OpenDSS application workshop 7 - Harmonic analysis, Electric Power Research Institute (EPRI), 3 Nov. 2009, Knoxville, TN.

[39] S. Herraiz, L. Sainz, and J. Clua, "Review of harmonic load flow formulations," *IEEE Transactions on Power Delivery*, vol. 18, Issue 3, pp. 1070-1087, July 2003.

[40] Anonymous, "Modeling and simulation of the propagation of harmonics in electric power networks. I. Concepts, models, and simulation techniques," *IEEE Transactions on Power Delivery,* vol. 11, no. 1, pp. 452,465, Jan. 1996.

[41] H. Sharma, W. G. Sunderman, A. Gaikwad, "Harmonic impacts of widespread use of CFL lamps on distribution systems," *IEEE Power and Energy Society General Meeting*, pp. 1-5, 24-29 July 2011.

[42] T. H. Ortmeyer, T. Hiyama, "Distribution system harmonic filter planning," *IEEE Transactions on Power Delivery*, vol. 11, no. 4, pp. 2005-2012, Oct. 1996.

[43] T. H. Ortmeyer, M. S. A. A. Hammam, T. Hiyama, D. B. Webb, "Measurement of the harmonic characteristics of radial distribution systems," *Power Engineering Journal*, vol. 2, no. 3, pp. 163-172, May 1988.

[44] A. Mansoor, W. M. Grady, AH Chowdhury, M. J. Samotyi, "An investigation of harmonics attenuation and diversity among distributed single-phase power electronic loads," *Transmission and Distribution Conference, Proceedings of the IEEE Power Engineering Society,* pp. 110-116, 10-15 Apr 1994.

[45] M. E. Balci, D. Ozturk, O. Karacasu, M. H. Hocaoglu, "Experimental verification of harmonic load models," *43rd International Universities Power Engineering Conference (UPEC),* pp. 1-4, 1-4 Sept. 2008.

[46] Anonymous, "Characteristics and modeling of harmonic sources-power electronic devices," *IEEE Transactions on Power Delivery,* vol. 16, no. 4, pp. 791-800, Oct. 2001.

[47] International Energy Agency, "Grid-connected photovoltaic power systems-survey of inverter and related protection equipments," Task V, Report IEA-PVPS T5-05:2002, Geneva Switzerland, December 2002.

[48] G. R. Ainslie-Malik, "Mathematical analysis of PWM processes," Doctoral Thesis, University of Nottingham, Nottingham UK, 2013.

[49] D. G. Holmes, "A general analytical method for determining the theoretical harmonic components of carrier based PWM strategies," *Proc. IEEE Industrial Applications Conf.,* pp. 1207 -1214, 1998.

[50] D. J. Kostic, Z. Z. Avramovic, N. T. Ciric, "A new approach to theoretical analysis of harmonic content of PWM waveforms of single- and multiple-frequency modulators," *IEEE Transactions on Power Electronics*, vol. 28, no. 10, pp. 4557-4567, Oct. 2013.

[51] M. Odavic, M. Sumner, P. Zanchetta, J. C. Clare, "A theoretical analysis of the harmonic content of PWM waveforms for multiple-frequency modulators," *IEEE Transactions on Power Electronics*, vol. 25, no. 1, pp. 131-141, Jan. 2010.

[52] Wilsun Xu, R. Bahry, H. E. Mazin, T. Tayjasanant, "A method to determine the harmonic contributions of multiple loads," *IEEE Power & Energy Society General Meeting, 2009*, pp. 1-6, 26-30 July 2009.

[53] K. Srinivasan, "On separating customer and supply side harmonic contributions," *IEEE Trans. on Power Delivery*, vol. 11, no. 2, 1996, pp. 1003-1012.

[54] H. Schau, A. Novitskiy, "Identification of the dominant harmonic source in the LV network on the base of anomalous power flows considerations," *2005 IEEE Russia Power Tech*, pp. 1-5, 27-30 June 2005.

[55] Zhiming Yin, Yuanyuan Sun, Tao Yu, "New methods exploration for harmonic source identification technologies," *4th International Conference on Electric Utility Deregulation and Restructuring and Power Technologies (DRPT)*, pp. 399-402, 6-9 July 2011.

APPENDIX A

GENERAL MATLAB CODE FOR HIGH FREQUENCY POWER FLOW STUDY

% To run the high frequency power flow for current injections by group B PV inverters at 16 kHz - Case I implementation (as described in Chapter 4).

%----------

```
clc;
clear all;
[DSSStartOK, DSSObj, DSSText] = DSSStartup;

if DSSStartOK
% Compile base circuit without solving
  DSSText.command='Compile (C:\Titiksha\RA\openDSS
\Master_fixed.dss)';

% Set up the interface variables
  DSSCircuit=DSSObj.ActiveCircuit;
  DSSSolution=DSSCircuit.Solution;

DSSText.Command ='New Energymeter.m LINE.LN1896_LN1897
enabled = True Terminal=2 Losses = YES';
DSSText.Command = 'Set Maxiterations=20';
DSSText.Command = ['set casename=Hfpf_f16kHz'] ;

% Edit the default harmonic spectrum
DSSText.Command='Spectrum.DEFAULTLOAD.NumHarm=1';
DSSText.Command='Spectrum.defaultvsource.NumHarm=1';
DSSText.Command='Spectrum.default.numharm=1';

% Define all the monitor objects
DSSText.Command='New Monitor.m2 Line.LN518_LN721';
DSSText.Command='new monitor.m5 Line.LN623_LN1480';
DSSText.Command='new monitor.m1 Line.LN1691_LN562';
DSSText.Command='new monitor.m3 Line.LN536_LN528';
DSSText.Command='new monitor.m4 Line.LN1124_LN1546';
DSSText.Command='new monitor.m6 Line.LN1749_LN522';
DSSText.Command='new monitor.c1 capacitor.cap_1914';
DSSText.Command='new monitor.c3 capacitor.cap_1404';

% Solve for power flow
DSSText.Command = 'solve ';
DSSText.Command = 'Sample';
DSSText.Command = 'Show Voltages LN Nodes'
DSSText.Command = 'Export Voltages '
DSSText.Command = 'Plot profile phases=all'
DSSText.Command = 'Show Lineconstants 60 mi'
```

```
DSSText.Command = 'Show Currents Elem Resid'
DSSText.Command = 'set harmonics=[200]';

% Calculate the fundamental currents for all PVs
DSSCircuit.SetActiveClass('Load')
iElement=DSSObj.Activeclass.First;
temp=0;LoadCurrents=cell(1,0);final=[]
while iElement>0
    temp=temp+1;
    LoadCurrents(temp,1) = {DSSCir-
cuit.ActiveCktElement.Currents}; %all the load cur-
rents
iElement = DSSObj.ActiveClass.Next;
end
temp=0;
for i=1003:1:1121
     temp=temp+1
     final=cell2mat(LoadCurrents(i,1))
    Ipv(temp)=0.03*abs(complex(final(1),final(2)));
end

% Define all the current sources at 16 kHz
DSSText.Command=['New Isource.scansource_' num2str(4)
' bus1=2158.1  phases=1 amps= '    num2str(Ipv(4)) '
angle=0 frequency=16000' ];
DSSText.Command=['New Isource.scansource_' num2str(10)
' bus1=2200.2  phases=1 amps= '    num2str(Ipv(10)) '
angle=0 frequency=16000' ];
DSSText.Command=['New Isource.scansource_' num2str(11)
' bus1=   2202.2  phases=1 amps= '    num2str(Ipv(11))
' angle=0 frequency=16000' ];
DSSText.Command=['New Isource.scansource_' num2str(12)
' bus1=   2212.2  phases=1 amps= '    num2str(Ipv(12))
' angle=0 frequency=16000' ];
DSSText.Command=['New Isource.scansource_' num2str(16)
' bus1=   2224.2  phases=1 amps= '    num2str(Ipv(16))
' angle=0 frequency=16000' ];
DSSText.Command=['New Isource.scansource_' num2str(17)
' bus1=   2228.2  phases=1 amps= '    num2str(Ipv(17))
' angle=0 frequency=16000' ];
.........
......
....
```

```
% Solve for harmonic solution
DSSText.Command = 'solve mode=Harmonics';
DSSText.Command = 'Save'
DSSText.Command = 'Show Voltage LN Nodes'
DSSText.Command = 'Show Currents Elem Resid'
DSSText.Command = 'Export voltages'
DSSText.Command = 'Export currents'

else
    a='DSS Did Not Start'
    disp(a)
end

%-----------------------------------------------------
```